Specificity and Mechanism of Coronavirus, Rotavirus and Mammalian Two-Histidine-Phosphoesterases That Antagonize Antiviral Innate Immunity

Abhishek Asthana[1], Christina Gaughan[1], Susan R. Weiss[2,3] and Robert H. Silverman[1,*]

[1]Department Cancer Biology, Cleveland Clinic Foundation, Lerner Research Institute, Cleveland, OH, 44195, United States; [2]Department of Microbiology, [3]Penn Center for Research on Coronaviruses and Other Emerging Pathogens, Perlman School of Medicine at the University of Pennsylvania, Philadelphia, PA, 19104, United States

* To whom correspondence should be addressed: Tel: 1-216-445-9650; Fax 1-216-445-6269; Email: silverr@ccf.org

ABSTRACT

2',5'-oligoadenylate(2-5A)-dependent endoribonuclease, RNase L, is a principal mediator of the interferon (IFN) antiviral response. Therefore, regulation of cellular levels of 2-5A is a key point of control in antiviral innate immunity. Cellular 2-5A levels are determined by IFN-inducible 2',5'-oligoadenylate synthetases (OASs) and by enzymes that degrade 2-5A. Importantly, many coronaviruses and rotaviruses encode 2-5A degrading enzymes thereby antagonizing RNase L and its antiviral effects. A-kinase anchoring protein 7 (AKAP7), a mammalian counterpart, could possibly limit tissue damage from excessive or prolonged RNase L activation during viral infections or from self double-stranded-RNAs that activate OAS. We show these enzymes, members of the two-histidine-phosphoesterase (2H-PE) superfamily, constitute a sub-family referred here as 2',5'-PEs. 2',5'-PEs from mouse coronavirus (CoV) MHV (NS2), MERS-CoV (NS4b), group A rotavirus (VP3), and mouse (AKAP7) were investigated for their evolutionary relationships and activities. While there was no activity against 3',5'-oligoribonucleotides, all cleaved 2',5'-oligoadenylates efficiently, but with variable activity against other 2',5'-oligonucleotides. The 2',5'-PEs are shown to be metal ion-independent enzymes that cleave trimer 2-5A (2',5'-p_3A_3) producing mono- or di-adenylates with 2',3'-cyclic phosphate termini. Our results suggest that elimination of 2-5A might be the sole function of viral 2',5'-PEs, thereby promoting viral escape from innate immunity by preventing or limiting the activation of RNase L.

IMPORTANCE

Viruses often encode accessory proteins that antagonize the host antiviral immune response. Here we probed the evolutionary relationships and biochemical activities of two-histidine-phosphoesterases (2H-PEs) that allow some coronaviruses and rotaviruses to counteract antiviral innate immunity. In addition, we investigated the mammalian enzyme, AKAP7, which has homology and shared activities with the viral enzymes and might reduce self-injury. These viral and host enzymes, that we refer to as 2',5'-PEs, specifically degrade 2',5'-oligoadenylate activators of the antiviral enzyme RNase L. We show that the host and viral enzymes are metal ion independent and exclusively cleave 2',5'- and not 3',5'-phosphodiester bonds, producing cleavage products with cyclic 2',3'-phosphate termini. Our study defines 2',5'-PEs as enzymes that share characteristic conserved features with the 2H-PE superfamily but which have specific and distinct biochemical cleavage activities. These findings may eventually lead to pharmacologic strategies for developing antiviral drugs against coronaviruses, rotaviruses, and other viruses.

INTRODUCTION

How interferons (IFNs) inhibit viral infections, and how viruses antagonize the IFN antiviral response, have been investigated for the past few decades, but with renewed intensity as a result of the SARS-CoV-2 pandemic (1-4). Mammalian cells often detect and respond to viruses after sensing viral double-stranded (ds)RNA, a common viral pathogen associated molecular pattern (PAMP) that induces type I and type III IFNs (1, 2). These IFNs induce expression of hundreds of IFN stimulated genes (ISGs), including numerous antiviral effector proteins (5). Included among the human antiviral proteins encoded by ISGs are 2',5'-oligoadenylate (2-5A) synthetases 1-3 (OAS1-3) consisting of one, two and three core OAS units, respectively (6-8). However, not all mammalian species express a similar set of homologous OASs, and some, but not all, related OASL proteins lack enzymatic activity (9, 10). Upon binding of, and activation by, viral dsRNA OAS1-3 synthesize 2-5A [$p_3(A2'p5')_nA$, where n=2 to >3] from ATP (7). The only known function of 2-5A is dimerization and activation of RNase L resulting in degradation of host and viral RNA, cessation of protein synthesis, apoptosis and inflammasome activation (11-15)(Fig. 1A). In addition to its antiviral effects, RNase L resulted in cell death in response to mutation of ADAR1 (adenosine deaminase acting on RNA-1) in a cell line or in cells treated with the DNA demethylating drug 5-aza-cytidine, both of which induce synthesis of self-dsRNA from repetitive DNA elements in the genome (16-18). Thus, regulation of 2-5A levels is critical for host cell viability as well as for control of viral infections and pathogenesis. Yet there are gaps in our knowledge of precisely how levels of 2-5A are established to restrict viral replication and

spread by RNase L activation while at the same time minimizing tissue damage to the host.

Regulation of 2-5A degradation is a key point of control in the OAS-RNase L pathway. Previously, we identified several different members of the eukaryotic-viral LigT group of the 2H-phosphoesterases (2H-PE) superfamily, named for two His- ϕ -Thr/Ser- ϕ motifs (where ϕ is a hydrophobic residue) that degrade 2-5A and therefore function as potent RNase L antagonists (19, 20) (Fig. 1B). Here we refer to 2H-PE members that degrade 2',5'-oligoadenylates as 2',5'-PEs. Other members of the 2H-PE superfamily have different activities, including 2',3'-cyclic nucleotide phosphodiesterase and 3',5'-deadenylase activities (19, 21).

The prototype of the 2',5'-PEs is the mouse coronavirus (CoV), mouse hepatitis virus (MHV), accessory protein NS2 (22). However, predicted or confirmed 2',5'-PEs are expressed by many betacoronaviruses (embecovirus lineage MHV, human coronavirus (HCoV) OC43, human enteric coronavirus (HECoV), equine coronavirus (ECoV), porcine hemagglutinating encephalomyelitis virus (PHEV) and merbeco lineage MERS-CoV and related bat CoVs), related toroviruses and group A and B rotaviruses (20, 23-26). However, the betacoronaviruses SARS-CoV and SARS-CoV-2 lack a 2',5'-PE. Perhaps as a consequence, SARS-CoV-2 activates, and is inhibited by, the OAS and RNase L pathway (4). In addition, there is also a mammalian 2',5'-PE, A-kinase anchoring protein (AKAP7, aka AKAP15 or AKAP18), that degrades 2-5A (27). Here we have expressed, purified and characterized the 2',5'-PEs from MHV (NS2), MERS-

CoV (NS4b), rotavirus group A (RVA) (VP3-C-terminal domain, CTD), and mouse AKAP7. We show that NS2 and NS4b are remarkably specific for cleaving 2',5'-linked oligoadenylates, whereas AKAP7 and VP3-CTD will also cleave other 2',5'-oligonucleotides. In contrast, all of the viral and mammalian 2',5-PEs tested lack the ability to cleave 3',5'-oligoribonucleotides. We further show that these enzymes are metal ion-independent and cleave trimer 2-5A (2',5'-p_3A_3) producing mono- and di-adenylates with 2',3'-cyclic phosphoryl termini. Our findings suggest that the sole function of the viral 2',5'-PEs may be to eliminate 2-5A allowing some coronaviruses and rotaviruses to evade the antiviral activity of RNase L.

RESULTS

Phylogenetic relationship and alignment of viral and cellular 2',5'-PEs.

To probe the precise molecular mechanism by which 2',5'-PEs allow some viruses to evade the antiviral effector RNase L, we further investigated MHV NS2, MERS-CoV NS4b, rotavirus group A (RVA) VP3-C-terminal domain (CTD), and mouse (mu)AKAP7, (Fig. 1B). A comparison of the domain organization of these 2',5'-PEs shows a related, catalytic domain. Some of these enzymes have additional domains related to intracellular localization, nucleic acid metabolism or protein binding functions indicative of their cellular compartment-specific or accessory functions (Fig. 1B). For instance, MERS-CoV NS4b and muAKAP7 contain N-terminal nuclear localization signal (NLS) domains (24, 27, 28). VP3 is a multifunctional enzyme that contains N-terminal guanylyltransferase (Gtase) and methyltransferase (Mtase) domains involved in capping

of the 5' termini of viral mRNAs (25, 29). muAKAP7 also has a carboxy-terminal binding domain for the regulatory subunit II (RII) of cyclic AMP (cAMP)-dependent protein kinase A (PKA-RII-α-BD) (27). In addition, MHV NS2 protein has a C-terminal extension of unknown identity or function (Fig. 1B).

To determine the phylogenetic relationships between the different 2',5'-PEs, we constructed a tree for amino acid sequences containing the catalytic domains from coronavirus, rotavirus and mammalian 2',5'-PEs (Fig. 2A). 2',5'-PEs were distributed into two distinct branches on the phylogenetic tree. VP3 group of proteins clustered into one branch while the other three groups containing NS2, NS4b and AKAP7 formed a separate branch (Fig. 2A). Within the VP3 group, RVA and RVB resolved on distinct sub-branches. Previously, full-length VP3 from RVA and RVB were also shown as separate distinct branches analogous to two separate clades (clade A and clade B) (30, 31). Interestingly, the NS2 proteins were mostly closely related to the mammalian AKAP7 catalytic domains, and then to the bat coronaviruses (HKU5 and SC2013) and MERS-CoV. The rotavirus VP3 proteins were most distally related to the other 2',5'-PEs.

Based on the phylogenetic relationship and functional relatedness, we further analyzed the sequence conservation by amino acid alignment. 2H-PE superfamily members are characterized by the presence of two H-ϕ-S/T-ϕ motifs, separated by an average of 80 amino acids (where ϕ represents a hydrophobic amino acid) (19). The alignment shows that both motifs are highly conserved across all 2',5'-PE proteins (Fig. 2B, see boxes).

These motifs form the catalytic core that bind to and cleave the 2-5A substrate. Consistent with the phylogenetic analysis, sequence analysis revealed that 2',5'-PEs clustered into four groups corresponding to NS2, NS4b, AKAP7 and VP3. The two histidines within the conserved motifs were 100% conserved among all the sequences (Fig. 2B, see asterisks). Several residues with intergroup consensus of >50% were identified in the alignment. The amino acid alignment shows several regions of conservation that exist beyond the two conserved catalytic motifs (H-ϕ-S/T- ϕ) (Fig. 2B, shown above sequence alignment).

Among the sequences in alignment, AKAP7 proteins of human, rat and mouse origin shared the highest amino acid identity ranging between 85 to 97% (88 to 97% similarity) (Table S1). NS2 proteins shared 48 to 92% identity (64 to 94% similarity), NS4b proteins shared 35 to 49% identity (50 to 69% similarity), and VP3 proteins shared 16 to 78% identity (29 to 84% similarity) within their groups. Interestingly while RVA VP3 proteins shared a high 78% identity (84% similarity) between them, they share only 16% identity (29% similarity) with the representative of RVB VP3 protein. The catalytic domains of 2',5'-PEs have modest intragroup alignment and a relatively lower intergroup alignment. Overall intergroup alignment for the catalytic domains of these proteins shown 10 to 22% identity (19 to 36% similarity) (Table S1). NS2 proteins shared 11 to 16% amino acid identity (24 to 29% similarity) with NS4b, 16 to 22% identity (30-36% similarity) with AKAP7 and 16 to 22% identity (26 to 32% similarity) with VP3 proteins. Similarly, NS4b group of proteins shared 12 to 18% identity (21 to 29% similarity) with AKAP7 and 10 to 19% identity (23 to 34% similarity) with VP3

proteins. AKAP7 and VP3 shared 11 to 20% identity and 19 to 25% similarity between the two groups.

2',5'-PEs are specific for 2',5'-linked phosphodiester bonds and preferably cleave 2',5'-oligoadenylate.

2',5'-PEs are members of the LigT family of the 2H-PE superfamily of enzymes, which are involved in RNA processing that can act on diverse substrates (19). Also, members such as MERS-CoV NS4b and muAKAP7 have a functional NLS peptide (24, 27). To determine if there was a wider role for these enzymes beyond cleaving 2-5A, we tested an expanded set of potential substrates. MERS-NS4b, MHV NS2, RVA VP3-CTD and muAKAP7 proteins were expressed in bacteria and then purified. Also, for comparison, human PDE12 (aka 2'-PDE), a member of the exonuclease-endonuclease-phosphatase (EEP) family known to cleave 2-5A was purified (Fig. 1B) (32, 33). The catalytically inactive mutant proteins, MERS-NS4b^{H182R}, MHV NS2^{H126R}, RVA VP3-CTD^{H718A}, muAKAP7$^{H93A;\ H185R}$ and human PDE12^{E351A} served as the negative controls. Purity and identity of trimer 2-5A (2',5'-p_3A_3) were confirmed by HPLC (Fig. 3A) and mass spectrometry [described later for (Fig. 5J)]. Purified 2',5,-PE proteins were incubated with 2-5A substrate at 30°C for 1 h and the 2-5A cleavage products analyzed by HPLC using a C18 column. All five wild type proteins cleaved 2-5A as observed by loss of intact 2-5A and appearance of peaks for the different cleavage products (Fig. 3B-F). Interestingly, MERS-NS4b (Fig. 3B) and MHV NS2 (Fig. 3C) degraded 2-5A to give two prominent products whereas RVA VP3-CTD (Fig. 3D) and muAKAP7 (Fig. 3E) gave four products upon extended degradation of 2-5A suggesting a difference in either

mechanism or rate of cleavage by these proteins. On the other hand, 2-5A cleavage by human PDE12 (Fig. 3F) results in the formation of two products corresponding to the elution time of the standard ATP and 5'-AMP, as previously described (32). As expected, the 2',5'-PE catalytically inactive mutant proteins containing a His-to-Arg or His-to-Ala mutations in the conserved histidines did not cleave 2-5A (Fig. 3G-J). Human PDE12 with Glu-to-Ala mutation at 351 amino acid residue also did not degrade 2-5A, as described previously (34) (Fig. 3K). Importantly, these findings show a different mode of 2-5A cleavage between 2',5'-PEs, members of the 2H-PE superfamily, and PDE12, a member of the EEP family of phosphodiesterases.

To investigate the expanded substrate specificity of 2',5'-PEs, we tested possible cleavage of various 2'-5' and 3'-5' linked oligoribonucleotides by HPLC. Purified 2',5'-PE proteins (1 µM) were incubated with either 2'-5'- or 3'-5'-linked pentaribonucleotide substrates (10 µM) at 30°C for 1 h. Wild type MERS-NS4b, specifically degraded 2'-5' p5'$(rA)_5$ by >99% while 2'-5' p5'$(rU)_5$, p5'$(C)_5$ or p5'$(G)_5$ were not degraded ($\leq$4%) (Table S2). Catalytically inactive mutant MERS-NS4b^{H182R} did not degrade any of the tested substrates under similar conditions. Wild type MHV NS2 also specifically degraded 2'-5' p5'$(rA)_5$ >99% while 2'-5' p5'$(rU)_5$, p5'$(C)_5$ or p5'$(G)_5$ were not degraded ($\leq$7%) (Table S2). Mutant MHV NS2^{H126R} did not degrade any of the tested substrates. These results suggest MERS-NS4b and MHV NS2 are remarkably specific in degrading 2'-5' linked oligoadenylate compared to the other substrates. We further tested RVA VP3-CTD which degraded 2'-5' p5'$(rA)_5$ >95%, p5'$(rU)_5$ ~ 40%, p5'$(C)_5$ ~90%, and p5'$(G)_5$ ~6% while mutant RVA VP3-CTD^{H718A} did not degrade any of the tested substrates (Table S2). Wild type muAKAP7 degraded 2'-5' p5'$(rA)_5$ >99%, p5'$(rU)_5$

228 >95%, p5'$(C)_5$ >95%, and p5'$(G)_5$ >90% while mutant muAKAP7$^{H93A;H185R}$ did not
229 degrade any of the tested substrates with the exception of 2'-5' p5'$(G)_5$ ~40% (Table
230 S2). To ensure that exclusive cleavage of 2',5'-oligoadenylates by MERS-NS4b was
231 not due to limiting amounts of enzyme, 10 µM of different 2',5'-linked penta-
232 ribonucleotides were incubated with three-fold higher concentrations (3 µM) of MERS-
233 NS4b at 30°C for 1h. Wild type MERS-NS4b specifically degraded 2'-5' p5'$(rA)_5$ >99%
234 while 2'-5' p5'$(rU)_5$, p5'$(C)_5$ or p5'$(G)_5$ were not degraded ($\leq$6%) suggesting MERS-
235 NS4b enzymatic activity is specific for degradation of 2',5'-oligoadenylates (Table S3).
236 Because MERS NS4b and MHV NS2 cleaved 2'-5' p5'$(rA)_5$ but not other 2'-5'-linked
237 substrates, we further determined if this was due to lack of binding to the other
238 substrates. To test this possibility, 10 µM of 2'-5' p5'$(rA)_5$ was incubated with 0.2 µM of
239 MHV NS2 in the absence or presence of increasing concentrations of 2'-5' p5'$(rU)_5$ at
240 30°C for 10 min. The amounts of 2'-5' p5'$(rA)_5$ degraded by MHV NS2 in the presence
241 of 0, 3.1, 10, 12.5, 25, 50 and 100 µM was determined by HPLC analysis (Fig. S1).
242 Degradation of 2'-5' p5'$(rA)_5$ by MHV NS2 decreased as the amount of 2'-5' p5'$(rU)_5$ in
243 the reaction increased beyond 10 µM (i.e. ratio >1:1) (Fig. S1). Our results suggests
244 that 2'-5' p5'$(rU)_5$ was able to bind MHV NS2 and competitively interfere with MHV NS2
245 ability to cleave 2'-5' p5'$(rA)_5$.

246 We next tested degradation activity of 2',5'-PEs against 3'-5' linked p5'$(rA)_5$, p5'$(rU)_5$
247 and p5'$(C)_5$. One µM of enzyme was incubated with 10 µM of the substrate at 30°C for 1
248 h. Wild type MERS-NS4b and its mutant MERS-NS4b^{H182R} , wild type MHV NS2 and its
249 mutant NS2^{H126R}, RVA VP3-CTD and its mutant RVA VP3-CTD^{H718A}, and wild type
250 muAKAP7 and its mutant muAKAP7$^{H93A;\ H185R}$ (Table S2) did not degrade the 3'-5'

linked substrates 3'-5' p5'$(A)_5$, 3'-5' p5'$(U)_5$, and 3'-5' p5'$(C)_5$. [We were unable to obtain 3'-5' p5'$(G)_5$ because of repeated failures of its chemical synthesis and/or purification, therefore this oligonucleotide could not be tested]. Our results suggest that all of the 2',5'-PEs examined are highly specific for cleaving 2',5' linked oligoribonucleotides. Among 2',5' linked substrates MERS-NS4b and MHV NS2, are specific for cleaving 2'-5' oligoadenylate, whereas RVA VP3-CTD cleaved in order: 2'-5' pA5>pC5>pU5>>pG5 and muAKAP7 cleaved all of 2',5' linked pentanucleotides with similar efficacy.

Based on the differential enzymatic activity of these 2',5'-PEs in degrading different types of 2',5'-linked phosphodiester substrates, we tested if they could degrade 2',3'-cyclic-GMP-AMP (cGAMP). cGAMP is a cyclic-dinucleotide secondary messenger with mixed phosphodiester linkages between 2'-OH of GMP to 5'-phosphate of AMP and 3'-OH of AMP to 5'-phosphate of GMP , synthesized by cyclic GMP-AMP-synthase (cGAS) in response to cytoplasmic dsDNA (35). cGAMP was incubated either with or without wild type and mutant 2',5'-PEs at 30°C for 1h and analyzed by HPLC. Wild type MERS-NS4b, MHV NS2, RVA VP3-CTD, and muAKAP7 did not degrade 2',3'-cGAMP whereas they did degrade 2',5'-p_3A_3 (served as a positive control) under similar conditions (Table S4). Catalytic mutants of 2',5'-PEs tested did not degrade 2',3'-cGAMP or 2',5'-p_3A_3 under similar conditions. The results suggest that 2',5'-PEs are capable of cleaving 2',5'-phosphodiester bonds in linear homo-ribonucleotides but not in the cyclic-mixed phosphodiester linked 2',3'-cGAMP.

2',5'-PEs exhibit metal ion-independent phosphodiesterase activity.

Metal ion dependency was evaluated by performing assays in either the presence of EDTA or magnesium. In the presence of EDTA, without added magnesium, 1 µM of MERS-NS4b (Fig. 4A) or MHV NS2 (Fig. 4B) degraded >90% of 2-5A in ~20 min whereas 0.05 µM of RVA VP3 CTD (Fig. 4C) and 1µM of muAKAP7 (Fig. 4D) degraded >90% of the 2-5A within 5 min. Relative rates of 2-5A degradation by RVA VP3-CTD >> muAKAP7 > MHV NS2 = MERS-NS4b were observed. Based on the specific activities, the ratio of fold activity of RVA VP3-CTD: muAKAP7: MERS-NS4b: MHV NS2 was 38.9: 2.9: 1: 1. It is noteworthy that many mammalian cell types have a total cellular Mg^{2+} concentration in between 17 to 20 mM, of which only 5-22% may be free depending on the cellular compartment. (36). We determined the specific activities of the 2',5'-PEs for degrading 2-5A in the absence and presence of 10 mM $MgCl_2$ at 5 min (Fig. 4E). The addition of Mg^{2+} ions decreased the specific activity of MERS-NS4b to ~0.6 fold and that of muAKAP7 to ~0.8 fold. The activity of MHV NS2 and RVA VP3-CTD showed a negligible decrease to 0.97 fold and 0.99 fold in the presence of Mg^{2+} ions, respectively. Our results suggest that the 2',5'-PEs activity of these proteins is independent of Mg^{2+} ions and its presence either slightly decreases or has no effect on the activity of these enzymes.

2',5'-PEs cleave 2',5'-linked oligoadenylate leaving products with cyclic 2',3' phosphoryl termini.

Differences in the 2-5A cleavage products as determined by HPLC (Fig. 3) suggested that viral and mammalian 2',5'-PEs cleave 2-5A via a different mechanism than human

296 PDE12, which degrades 2-5A to produce ATP and AMP (32). Among 2',5'-PEs, MERS-
297 NS4b and MHV NS2 degraded 2-5A to give two cleavage products whereas RVA VP3-
298 CTD and muAKAP7 gave four cleavage products. Therefore we decided to determine
299 the precise cleavage sites in 2-5A by 2',5'-PEs. 2-5A was partially digested with MERS-
300 NS4b (Fig. 5) or RVA VP3-CTD (Fig. 6) followed by the collection of individual peak
301 fractions of cleavage products. Cleavage products were subsequently identified and
302 confirmed by HPLC analysis (comparing elution time with known standards),
303 identification by m/z ratio (LC/MS/MS analysis of collected peaks) or biochemical
304 analysis (by 5'-dephosphorylation) (Figs. 5A & 6A).
305
306 Partial digestion of 2-5A by MERS-NS4b was confirmed by HPLC analysis of the
307 samples using a C18 column (Fig. 5B) and comparing it with the chromatogram of intact
308 2-5A (Fig. 3A). The partially digested 2-5A by MERS-NS4b was run on a Dionex
309 DNAPac^{R}PA-100 column in an ammonium bicarbonate volatile buffer system as
310 described in Methods. Individual peaks were collected and processed for mass
311 spectrometry analysis. Individually collected peaks were also rerun on a C18 column to
312 confirm the purity and matched elution times of the collected peaks before performing
313 LC/MS/MS (Figs. 5C, D). Mass spectrometric analysis of the peaks revealed an m/z
314 ratio of 597.25 (Fig. 5H) and 570.4 (Fig. 5I). The m/z ratios of 597.25 and 570.4 were
315 compared to the masses of potential 2-5A degradation/intermediate products (Fig. 5G)
316 and were found to correspond to ApA and p_3A>p (where ">p" represents a 2',3' cyclic
317 phosphate), respectively. Intact 2-5A gave an m/z ratio of 584 for the double charged
318 ion (Fig. 5J). Moreover, the collected peak of p_3A>p (shown in Fig. 5D) was subjected to

SAP mediated 5' dephosphorylation which results in the peak corresponding to A>p (Fig. 5E, F). This experiment suggested that MERS-NS4b degrades 2-5A to produce a 5'-product with 2',3' cyclic phosphate terminus in the form of p_3A>p and a 3'-product of ApA. To test if p_3A>p and ApA are end products of the reaction, we subjected 2-5A to extended degradation by MERS-NS4b and monitored the area under the peak corresponding to ApA at 0 h, 1 h, 4 h and 24 h (Fig. S2 A-D, I). After the ApA peak appears (at 1h) its amount remained unchanged up to 24 h. Also, 2'-5' linked 5'pApA incubated with MERS-NS4b did not result in any degradation (Fig. S2 E-H, I). These results suggest that MERS-NS4b does not cleave di-adenylates into smaller products irrespective of 5' mono-phosphorylation status under the given experimental conditions.

With a similar approach, we designed an experiment to elucidate the cleavage products and intermediates formed upon 2-5A degradation by RVA VP3-CTD (Fig. 6A). Because RVA VP3-CTD has high specific activity against 2-5A (Fig. 4), 2-5A was incubated with decreased protein concentrations and times of incubation to capture any possible intermediates and degradation products of 2-5A (Fig. 6B, C). 2-5A cleaved by VP3-CTD forms products which based on the elution times of the known standards and compounds were identified as p_3A>p, A>p, ApA, adenosine and an unknown intermediate (shown in grey color) (Fig. 6C). Based on potential degradation intermediates we speculated the unknown intermediate to be p_3ApA>p. To test this possibility, a part of the sample reaction with 2-5A cleavage products (obtained from the sample used in Fig. 6C) was subsequently treated with SAP to remove 5'-phosphorylation from cleavage products (if any) which would result in the formation of

A>p and ApA>p from p_3A>p and p_3ApA>p, respectively (Fig. 6E). The dephosphorylated sample was analyzed by running it on a C18 column. After SAP treatment, the amount of adenosine and ApA remained constant when compared before (Fig. 6C) and after (Fig. 6D) dephosphorylation, as calculated by integrating the area under the peaks of the HPLC chromatograms. However, the total area under the peak corresponding to A>p increased suggesting A>p was formed as a result of dephosphorylation of p_3A>p (Fig. 6C, D). Importantly, a new peak (possibly ApA>p) appears which is formed by dephosphorylation of an unknown intermediate (Fig. 6D, shown in grey color). The dephosphorylated samples were run on a Dionex DNAPac^R PA-100 column in an ammonium bicarbonate volatile buffer system as described in the Methods. Individual peak fractions were collected and processed for mass spectrometry analysis. Collected peaks were rerun on a C18 column to confirm the purity and match the elution time of the collected peak with that of A>p and 'dephosphorylated intermediate' (Fig. 6D) before performing LC/MS/MS. Mass spectrometric analysis of the peaks revealed m/z ratios of 330 corresponding to A>p (Fig. 6F) and 659.1 which corresponds to that of ApA>p (Fig. 6G). This experiment suggests that trimer 2-5A (2',5'p_3A_3) degradation by RVA VP3-CTD proceeds via formation of p_3ApA>p and ApA intermediates. RVA VP3-CTD degrades p_3ApA>p to form p_3A>p (5'-product) and A>p (3'-product) whereas di-adenylate (ApA) is further degraded to yield A>p (5'-product) and adenosine (3'-product). Complete degradation of p_3A_3 by RVA VP3-CTD results in the formation of p_3A>p, A>p and adenosine as end products (Fig. 3D). Further, the preferred site of p_3A_3 cleavage by RVA VP3-CTD was investigated in a time-course experiment. RVA VP3-CTD (0.05 µM) was incubated with p_3A_3 (200 µM) substrate at 30°C and samples were

collected at different time points. The substrate or product peaks at each time point were analyzed by calculating the percent of the area under the peaks of the HPLC chromatograms (Fig. S3) and tabulated (Fig. S4A). The analysis revealed that the majority of p_3A_3 is cleaved by RVA VP3-CTD to produce p_3ApA>p (5'-product) and adenosine (3'-product). The intermediate species (p_3ApA>p) is subsequently cleaved to produce p_3A>p (5'-product) and A>p (3'-product). A minor fraction of p_3A_3 is cleaved by RVA VP3-CTD to produce p_3A>p (5'-product) and ApA (3'-product). The di-adenylate intermediate (ApA) is subsequently cleaved into A>p (5'-product) and adenosine (3'-product) (Fig. S4B), which is apparent from incubations at a higher concentration of RVA VP3-CTD (Fig. 3D). Moreover, the degradation pattern of the two di-adenylate intermediates reveals that tri-phosphorylated intermediate (p_3ApA>p) is readily cleaved by RVA VP3-CTD whereas ApA cleavage is slow suggesting 5'-tri-phosphorylated molecules are preferred over non-phosphorylated substrates (Figs. S3, S4). In a separate experiment, 10 µM of 2'-5' linked 5'$p(A)_2$ was incubated with 1 µM of VP3-CTD at 30°C for 1 h. The results confirmed the formation of cleavage products corresponding pA>p (5'-product) and adenosine (3'-product) (Fig. S5). Moreover, in another time-course experiment muAKAP7 cleaved p_3A_3 to produce p_3A>p (5'-product) and ApA (3'-product) (Fig. S6). The ApA intermediate was further cleaved to form A>p and adenosine. Interestingly, unlike RVA VP3-CTD, muAKAP7 mediated cleavage of p_3A_3 does not form p_3ApA>p intermediate.

Overall mechanisms and differences in degradation of 2-5A by representative EEP (PDE12) and 2',5'-PEs family members are summarized in figure 7. Human PDE12 degrades trimer 2-5A into ATP and 2 (5'-AMP)s in the presence of Mg^{2+} ions, as has

been reported (32). On the other hand, mammalian and viral 2',5'-PEs, act in a metal-ion independent way, degrading 2-5A to form 5' products with 2',3' cyclic phosphates. All 2',5'-PEs quickly cleave active anti-viral 2-5A into inactive molecules that is, the products are not capable of activating RNase L because of a requirement for at least three adenylyl residues (37). MERS-NS4b and MHV NS2 degrade trimer 2-5A to form p_3A>p and ApA. RVA VP3-CTD and muAKAP7 further cleave ApA to form A>p and adenosine as products. In addition to the above-mentioned degradation intermediates and products of 2-5A, RVA VP3-CTD also produced p_3ApA>p as an intermediate, suggesting it to be a 2',5'-specific endoribonucleolytic phosphodiesterase (Figs. 6 & 7).

DISCUSSION

Cleavage specificity and mechanism of 2',5'-PEs

The 2',5'-PEs studied here exclusively cleaved 2',5'- and not 3',5'-phosphodiester bonds. There was also a strong preference for cleavage of 2',5'-oligoadenylates by NS2 and NS4b and, to a lesser extent, by VP3-CTD, whereas AKAP7 had similar activities against the different 2',5'-linked pentamers of A, U, C and G. Therefore, although AKAP7 and VP3-CTD are not the mostly closely related 2',5'-PEs, they can both cleave 2',5'-oligoribonucleotides other than 2-5A (Fig. 2A and Table S2). Interestingly, OASs are 2'-nucleotidyl transferases that not only use ATP as substrates but can produce diverse molecules with 2',5' linkages. NAD^+, tRNAs, A5'$p_4$5'A, and mono- and poly-ADP-ribose are acceptors for addition of 2',5'-AMP residues from ATP by OAS. Also,

OAS can add other 2'-terminal ribo- and deoxy-nucleotide monophosphates to 2-5A (38-41). However, which, if any, of these alternative 2-5A-like molecules can be cleaved by 2',5'-PEs remains to be determined. The cGAMP, a cyclic dinucleotide that activates STING, has one 2',5'-linkage and one 3',5'-linkage, but it is not cleaved by the 2',5'-PEs examined here (Table S4). VP3 was phylogenetically distal and has the most distinct mechanism of 2-5A cleavage compared to all of the tested 2',5'-PEs. It is also interesting to note that the two coronavirus 2',5'-PEs (NS4b and NS2) are less closely related than NS2 is to the host enzyme, AKAP7 (Fig. 2A & Table S1). Our results suggest that the main, and perhaps only, function of these activities is to degrade 2-5A thus preventing RNase L activation and viral escape, or in the case of AKAP7 reducing cell and tissue damage from RNase L activity. These 2',5'-PEs are also metal ion independent enzymes, as is RNase L (42).

The viral and mammalian 2',5'-PEs produce cleavage products from trimer 2-5A (2',5'-p_3A_3) with cyclic 2',3'-phosphoryl groups, and not 2',3'-OH termini. These conclusions are based on analysis of 2-5A cleavage products by two types of HPLC columns (Dionex and C18) and, importantly, by mass spectrometry. In contrast, our prior studies based on more limited analysis of the 2-5A cleavage products by one type of HPLC column (Dionex) misidentified these cleavage products of NS2, VP3-CTD, and AKAP7 as AMP and ATP (22, 25, 27).

Interestingly, mammalian and viral 2',5'-PEs have activities highly similar to an invertebrate 2H-PE present in the oyster, Crassostrea gigas (43). The oyster enzyme

has sequence similarity to AKAP7, is metal ion independent, cleaves 2',5'- but not 3',5'-linked oligonucleotides, and leaves cyclic 2',3'-phosphate and 5'-OH termini on its products. It also degraded tri-phosphorylated 2-5A oligomers with multi-fold efficiency compared to the corresponding non-phosphorylated core 2-5A oligomers. Similarly, we observed RVA VP3-CTD degrades 5'-triphosphorylated-di-adenylate with 2',3' cyclic phosphoryl termini (p3ApA>p) preferentially compared to the non-phosphorylated di-adenylate (ApA) core molecule (Figs. S3 & S4). However, the function and role of 2-5A cleaving enzymes in invertebrates is still unknown.

It is also unknown if the 2',3'-cyclic phosphates on 2-5A breakdown products generated by 2',5'-PEs have cell signaling functions. However, small self RNAs with 2',3'-cyclic phosphate termini (generated by RNase L) induced IFN-β expression through RIG-I, MDA5, and MAVS (44). Additionally, RNase L-cleaved RNA with 2',3'-cyclic phosphates stimulated the NLRP3 inflammasome leading to IL-1β secretion (15). Also, during *Staphylococcus aureus* infections RNase T2 cleaves ssRNA producing purine-2',3'-cyclic phosphate terminated oligonucleotides sensed by TLR8 (45). The mammalian enzyme USB1, another 2H-PE, also produces 2',3'-phosphoryl temini during deadenylation of U6 snRNA, but it clearly differs from the 2',5'-PEs because it cleaves 3',5'-phosphodiester bonds (21).

2-5A catabolism during the IFN induced cellular responses to viral and host dsRNA.

The ability of viruses to evade or antagonize the IFN response contributes to viral tropism and disease pathogenesis. Accordingly, viruses have evolved or acquired diverse strategies to overcome inhibition by type I and type III IFNs, both of which induce transcription of OAS genes (1, 2, 46). However, the precise cellular and molecular mechanisms by which viruses impede tissue specific host defenses leading to virus-induced pathology continue to be investigated. With regard to the OAS-RNase L pathway, it is the balance between 2-5A anabolic (OAS) and catabolic (e.g. 2',5'-PEs and PDE12) (20) activities that determine whether virus replication is blocked by RNase L. For instance, RNase L fails to inhibit coronaviruses MHV and MERS-CoV, or rotaviruses, unless there is an inactivating mutation of their 2-5A degrading enzymes (NS2, NS4b, and VP3, respectively) (22, 24-26). In contrast, SARS-CoV-2, which lacks a gene for a similar protein, is inhibited by RNase L (4). In this context, enzymes that degrade 2-5A, such as PDE12, are drug targets in the hunt for broad spectrum antiviral agents (32, 47).

The viral enzymes NS2, NS4b and VP3-CTD are antagonists of innate immunity that support virus replication by eliminating 2-5A and preventing, or reducing, activation of RNase L by 2-5A (20, 22, 24-26). In contrast, mammalian AKAP7 is a nuclear 2',5'-PE that does not affect viral replication, unless its nuclear localization signal peptide is deleted leading to cytoplasmic accumulation (27). A mutant AKAP7 deleted for its N-terminal nuclear localization signal peptide accumulates in the cytoplasm was able to rescue an NS2 mutant of MHV (22). While the function of the 2',5'-oligonucleotide

cleaving activity of AKAP7 is still unresolved, the phylogenetic tree suggests that the NS2 coronavirus proteins may have evolved from the AKAP7 catalytic domain (Fig. 2A).

Enzymes that degrade 2-5A have significance beyond antiviral innate immunity. Self-dsRNA activates the OAS-RNase L pathway leading in some circumstances to apoptosis (12,13). In one example, mutation or inhibition of the dsRNA editing enzyme, ADAR1, leads to accumulation of self dsRNA activating OAS-RNase L leading to cell death, and PKR, inhibiting protein synthesis initiation (16, 48). In another instance, DNA methyltransferase inhibitors, e.g. 5-aza-cytidine, cause self-dsRNA accumulation from repetitive DNA elements leading to OAS-RNase L activation and apoptosis (17, 49). Thus, 2-5A is a secondary messenger for cytotoxic and antiviral activities of either non-self (viral) or self-dsRNA (host) whose levels must be tightly controlled to limit cytotoxicity while restricting viral spread. Our findings provide a mechanistic understanding of how 2',5'-PEs regulate 2-5A levels among coronaviruses MHV, MERS-CoV, and group A rotaviruses and in mammalian cells through the activity of AKAP7 (22, 24, 25, 27), with implication for both control of virus replication and cellular responses to self-dsRNA. Furthermore, our study defines 2',5'-PEs as a new sub-group within the 2H-PE superfamily that shares characteristic conserved sequence features of the superfamily but with specific and distinct biochemical cleavage activities. Knowledge derived from the study of these 2-5A degrading enzymes could lead to future avenues of antiviral drug development.

MATERIAL AND METHODS

cDNA cloning and plasmids.

Human PDE12 cDNA was PCR amplified (using DNASU cDNA clone HsCD00296464 in vector pDONR221, GenBank: NM_177966.5) with forward primer 5'-TTCAAgaattcATGTGGAGGCTCCCAGGCGC-3' (with an EcoRI restriction site) and the reverse primer 5'-TTCAAgtcgacTCATTTCCATTTTAAATCACATACAAGTGCTATGTGATC-3' (with a SalI restriction site). $PDE12^{E351A}$ pGEX 6P-1 mutant (34) plasmid was constructed by MegaPrimer method (50) using mutagenic reverse primer 5'-GCGCGGTCAACCgCCTGCAAACAG-3'. The amplified wild type and mutant PDE12 cDNAs were cloned into plasmid pGEX-6P-1 (GE Healthcare, USA) at the EcoRI and SalI restriction site, sequenced and expressed in E. coli as glutathione *S*-transferase (GST) fusion proteins. To subclone the VP3 C-terminal domain (CTD) cDNA of rotavirus A strain RVA/Simian-tc/USA/RRV/1975/G3P (GenBank: EU636926.1) and its H718A mutant, we used codon-optimized constructs for expression in Sf9 insect cells (GenBank: KJ869109.1) (30) (gifts from Kristin Ogden, Vanderbilt University). The cDNAs were PCR amplified and cloned into plasmid pMAL-C5X at the XmnI (blunt cloned) and NcoI (sticky end) restriction site. Blunt end forward primer 5'-TACGCTGACGACCCCAACTACTTCATCG-3' and reverse primer 5'-TTCAAccatggTTATTACTCGGACATGTCGAACACGGTGTCG-3' with NcoI restriction site were used for VP3-CTD. The wild type and H718A RVA VP3-CTD proteins were expressed fused to maltose binding protein (MBP). Additional protein expression plasmid constructs were previously described with sequences originating from MERS-

525 CoV (MBP-NS4b and its mutant MBP-NS4b^{H182R}) (24); from MHV (MBP-MHV NS2 and
526 its mutant MBP-NS2^{H126R}) (22), and mouse AKAP7 and its mutant AKAP7$^{H93A; H185R}$ (27).
527
528 **Protein expression and purification**
529 Proteins were expressed from pGEX-6P-1 or pMAL constructs in E. coli strain
530 BL21(DE3)/pLysS (Life Technologies, USA). Wild type and catalytically inactive
531 mutants of AKAP7 and PDE12 were expressed as GST-fusion proteins and purification
532 was performed by modification of a previous protocol (51). Single colonies were used to
533 inoculate primary cultures which were subsequently used to seed secondary cultures
534 grown to 0.6 OD (600 nm) in a shaking incubator at 37°C and 250 rpm. Cells were
535 induced with 0.2 mM IPTG, for 16 h at 22°C. Induced cell pellets were re-suspended in
536 buffer A [20 mM HEPES pH 7.5, 1 M KCl, 1 mM EDTA, 10% glycerol v/v, 5 mM DTT
537 and EDTA-free Pierce™protease inhibitor (Thermo Scientific, USA)]. Pelleted cells were
538 lysed by addition of 200 µg/ml lysozyme followed by sonication. Supernatants were
539 collected after centrifugation at 12,000x g, 40 min, 4°C in a Beckman JA-17 rotor.
540 Supernatants were added to Pierce™ Glutathione Agarose (Thermo scientific, USA)
541 and incubated for 2 h at 4°C followed by washes with buffer A. Digestions to release the
542 GST tag were performed with PreScission Protease (Cytiva, USA) in 50 mM Tris-HCL
543 pH 7.5, 150 mM NaCl, 1 mM EDTA, and 1 mM DTT for 16 h at 4°C. Supernatants
544 containing untagged protein were concentrated using Centriprep centrifugal filter
545 devices (Millipore; molecular weight cutoff, 10 kDa) and loaded on superdex 75 column
546 on an AKTA pure 25L protein purification system (GE Healthcare, USA) in 20 mM
547 HEPES pH 7.5 150 mM NaCl, and 1 mM DTT. Wild type and mutant RVA VP3-CTD

548 expressing bacterial culture growth and IPTG induction conditions were same as
549 described above, except that growth media additionally included 2% glucose. Harvested
550 bacterial cell pellets were suspended in Buffer B [20 mM Tris-HCl pH 7.4 with 200 mM
551 NaCl, 1mM EDTA, 10 mM β-mercaptoethanol, EDTA free protease inhibitor (Pierce™
552 Protease inhibitor, Thermo Scientific, USA) and 10% glycerol] and lysed with lysozyme
553 followed by sonication. Supernatants were incubated with Amylose resin (NEB, USA),
554 washed three times with buffer followed by elution with 100 mM maltose. Proteins were
555 concentrated using Centriprep centrifugal filter devices (Millipore; molecular weight
556 cutoff, 10 kDa) and further purified using size exclusion chromatography (SEC) on an
557 AKTA pure 25L protein purification system (GE Healthcare, USA) in buffer C (20 mM
558 HEPES pH 7.5, 100 mM NaCl and 1 mM DTT). Wild type and catalytic mutants of
559 NS4b, and MHV NS2 were purified as described previously (22, 24). In addition to
560 inactive mutants, purified MBP protein was used as control in experiments with MBP
561 fusion proteins. Protein concentrations were determined using Bio-Rad protein assay
562 reagent (Bio-Rad, USA). All proteins were stored in Buffer C supplemented with 10%
563 glycerol in -80°C.
564
565 **Synthesis and purification of 2-5A oligomers and other oligoribonucleotide**
566 **substrates**
567 2-5A or $p_3$5'A(2'p5'A)$_2$ (2',5'-p_3A_3) was synthesized from ATP by using histidine-tagged
568 porcine-OAS1 (52). The OAS was immobilized and activated with poly(I):poly(C)-
569 agarose (53). Briefly, poly(I):poly(C)-agarose beads were washed with buffer D [10 mM
570 HEPES pH 7.5, 1.5 mM $Mg(CH_3COO)_2.4H_2O$, 50 mM KCl, 20% glycerol, and 7 mM β-

mercaptoethanol]. Ten ml of beads were incubated with 10 mg of purified OAS protein for 2 h at 25°C with intermittent vortexing. Beads were washed three times with buffer D by centrifugation at 3000 g at 4°C for 30 min. Beads were suspended in the reaction mixtures containing 20 mM HEPES pH 7.5, 20 mM $Mg(CH_3COO)_2.4H_2O$, 20 mM KCl, 1 mM EDTA and 10 mM ATP. The reaction mixtures were incubated in a shaking incubator set at 37°C, 120 rpm for 18 h. The supernatant was collected by centrifugation at 3000 g at 4°C for 30 min. The supernatant was heated at 95°C for 5 min and again centrifuged at 18,000 g for 15 min at 4°C to remove the precipitate. To isolate individual 2-5A oligomers, the supernatant containing crude, unfrationated 2-5A oligomers were run on an HPLC (1260 Infinity II Agilent technologies) equipped with a preparative Dionex column (BioLC^{R}DNAPac^{R}PA-100, 22 x 250 mm, Dionex, USA). Samples were injected and elution performed at a flow rate of 3 ml/min in a stepwise gradient of 10-400 mM (0-120 min), 400-800 mM (121-125 min) and 10 mM (126-160 min) of NH_4HCO_3 buffer (pH 7.8). Fractions were collected, lyophilized and suspended in nuclease-free water.

RNA oligoribonucleotides (other than 2',5'-p_3A_3) with 2'-5' or 3'-5' phosphodiester linkages were commercially purchased. Oligonucleotide substrates 5'-pA2'p5'A2'p5'A2'p5'A2'p5'A -3' , 5'-pU2'p5'U2'p5'U2'p5'U2'p5'U -3', 5'-pG2'p5'G2'p5'G2'p5'G2'p5'G -3', 5'-pA3'p5'A3'p5'A3'p5'A3'p5'A -3', 5'-pU3'p5'U3'p5'U3'p5'U3'p5'U -3' were purchased from Integrated DNA Technologies (IDT, USA) while 5'-pC2'p5'C2'p5'C2'p5'C2'p5'C -3', 5'-pC3'p5'C3'p5'C3'p5'C3'p5'C -3' and 5'-pA2'p5'A -3' were purchased from ChemGenes Corporation (Wilmington, USA).

Penta-ribonucleotides substrates are shown as p5'$(rN)_5$, where N represents A, U, G, or C nucleotide. A2'p5'A standard was prepared by incubating 5'pA2'p5'A with shrimp alkaline phosphatase (ThermoFisher, USA) as per manufacturer's protocol. 2',3'-cyclic-GMP-AMP (cGAMP), ATP, AMP and adenosine were obtained from Sigma Aldrich, USA.

Phosphodiesterase activity assays

Ten µM of the substrates (with either 2'-5' or 3'-5' phosphodiester linkage) were incubated with 1 µM of enzyme. Final reactions were performed in 20 mM HEPES buffer pH 7.4, 1 mM DTT and 10 mM $MgCl_2$ by incubating at 30°C for 1 h (or for the time indicated in the text). Where indicated, reactions were performed in the absence of $MgCl_2$ with 2 mM EDTA added. Reactions were stopped by heating at 95°C for 5 min. Samples were centrifuged at 18,000 g for 15 min at 4 °C. Supernatants were collected and analyzed by HPLC. 2',3'-cGAMP degradation assays were performed and analyzed using the same conditions as described above. In all experiments, substrates incubated under similar conditions in the absence of enzyme served as control.

HPLC analysis and identification of products

The substrates and cleavage products were analyzed on a 1260 Infinity II Agilent technologies HPLC equipped with an Infinitylab Poroshell 120 C18 analytical column (Agilent technologies, 4.6 x 150 mm, 4µm). Eluent A was 50 mM ammonium phosphate buffer pH 6.8 and eluent B was 50% methanol in water. Five µl of processed samples were injected on the C18 column, at a flow rate of 1 ml/min and eluted with a linear

gradient (0-40%) of eluent B over a period of 20 min, then 3 min 40% Eluent B, followed by equilibration to initial condition (100% Eluent A). The HPLC column was maintained at 40°C. Spectra were recorded at 256 nm. The products were identified either by comparing the elution time of known standards or by mass-spectrometry analysis. Alternatively, to test expanded substrate specificity, 10 µl of processed samples were injected on a Dionex DNAPac^{R}PA-100 analytical column at a flow rate of 1 ml/min and eluted with a linear gradient of 10-800 mM of NH_4HCO_3 buffer (pH 7.8) over a period of 90 min, followed by 30 min equilibration to initial condition. Open Lab CDS software was used to analyze and calculate area under the peaks in HPLC spectra.

Shrimp Alkaline phosphatase (SAP) mediated phosphorylation analysis

Purified substrates and cleavage product mixtures were dephosphorylated by incubating with SAP (ThermoFisher, USA) at 37°C for 1 h according to the manufacturer's protocol. Samples were prepared for subsequent analysis as described above.

Sample preparation for mass spectrometry

Desired peak fractions (including cleavage products of 2',5'-p_3A_3) were collected by running samples on a Dionex DNAPac^{R}PA-100 analytical column as described above. Collected peaks were subjected to acetone precipitation, supernatants containing cleavage products (from HPLC peak) were collected and lyophilized. Lyophilized samples were suspended in 1 mM NH_4HCO_3 buffer (pH 7.8) and used for mass spectrometry analysis.

640

641 **Mass spectrometry analysis of cleavage products**

642 Prepared samples were subjected to mass spectrometry analysis. The LC/MS/MS
643 analysis was carried out using a triple quadrupole tandem mass spectrometer (TSQ-
644 Quantiva, Thermo Scientific, USA) equipped with an electrospray ionization (ESI)
645 interface. The mass spectrometer was coupled to the outlet of HPLC system that
646 consisted of an UHPLC system (Vanquish, Thermos Fisher Scientific, USA), including
647 an auto sampler with refrigerated sample compartment and inline vacuum degasser.
648 The Xcalibur software was used for data processing. The ESI mass spectrometric
649 detection was performed in both the negative and positive ionizations, with ions spray
650 voltage at 2.5kV, sheath gas at 35 Arb and Aux gas at 20 Arb. The ion transfer tube
651 and vaporizer temperatures were set at 350°C and 250°C, respectively. The qualitative
652 analysis was performed using full scan at the range from 200 to 1250 (m/z). Five µl
653 extracted samples were injected on the C18 column (Gemini, 3 µm, 2 x 150 mm,
654 Phenomenex, CA) with the flow rate of 0.3 ml/min at 45°C. Mobile phases were A
655 (water containing 10 mM ammonium acetate and 20 mM ammonium hydroxide) and B
656 (methanol containing 10 mM ammonium acetate and 20 mM ammonium hydroxide).
657 Mobile phase B at 0% was used at 0-2 min, a linear gradient was used starting from 0%
658 B to 100% B at 2-12 min, kept at 100% at 12-26 min, then from 100% B to 0% B at 26-
659 27 min and kept at 0% B for 8 min. The peaks shown in full scans were processed to
660 locate and identify the cleavage products of the 2',5'-p_3A_3 substrate using the Xcalibur
661 software v4.1. Standard adenosine, AMP, ATP and adenosine-2',3'-cyclic
662 monophosphate sodium salt were run for reference.

663

664 **Bioinformatic Analysis**

665 The PDE domain sequences from different 2',5'-PEs were used for creating a multiple
666 sequence alignment using MAFFT version 7 (54) employing iterative refinement method
667 E-INS-I (https://mafft.cbrc.jp/alignment/server/). The MAFFT sequence alignment result
668 was downloaded in clustal format and visualized using Jalview 2.11.1.3 software. The
669 sequence alignment was further processed on MAFFT server to calculate the
670 phylogenetic tree using neighbor joining method and JTT substitution model and then
671 visualized tree using Archaeopteryx.js software. The resultant fasta format output of
672 MAFFT multiple sequence alignment was used to calculate the percentage of amino
673 acid identity and similarity by Sequence Identity and Similarity (SIAS) tool with default
674 parameters (http://imed.med.ucm.es/Tools/sias.html).The name, accession number
675 and amino acid (aa) region of the aligned sequences are MHV NS2 (UniProtKB/Swiss-
676 Prot: P19738.1, aa 41-135), Human coronavirus (HCoV) OC43 NS2 (GenBank:
677 AAT84352.1, aa 43-138), Human enteric coronavirus (HECoV) NS2 (GenBank:
678 ACJ35484.1, aa 39-140), Equine coronavirus (ECoV) NS2 (GenBank: ABP87988.1, aa
679 42-140), Middle East respiratory syndrome coronavirus (MERS-CoV) NS4b (GenBank:
680 AFS88939.1, aa 87-191), Rat AKAP7 δ/γ (NCBI RefSeq: NP_001001801.1, aa 121-
681 233), Mouse AKAP7 isoform-1 (NCBI RefSeq: NP_061217.3, aa 82-194), Human
682 AKAP7 γ (NCBI RefSeq: NP_057461.2, aa 100-233), Human rotavirus group A (RVA)
683 WA-VP3 (GenBank: AFR77808.1, aa 707-806), Simian rotavirus group A (RVA) SA11-
684 N5 (GenBank: AFK09591.1, aa 707-808), Human rotavirus group B (RVB) Bang117
685 (GenBank: ADF57896.1, aa 655-750), Bat coronavirus (BtCoV) SC2013 NS4b

(GenBank: AHY61340.1, aa 96-195) and Bat coronavirus (BtCoV) HKU5 NS4b (NCBI RefSeq: YP_001039965.1, aa 91-192).

AVAILABILITY

Multiple sequence alignment software is available (https://mafft.cbrc.jp/alignment/server/). Alignment and phylogenetic tree construction tool is downloadable (https://www.jalview.org/). Sequence Identity and Similarity (SIAS) tool with default parameters is available (http://imed.med.ucm.es/Tools/sias.html).

ACCESSION NUMBERS

The name and accession number of the aligned sequences are MHV NS2 (UniProtKB/Swiss-Prot: P19738.1), HCoV OC43 NS2 (GenBank: AAT84352.1), HECoV NS2 (GenBank: ACJ35484.1), ECoV NS2 (GenBank: ABP87988.1), MERS-CoV NS4b (GenBank: AFS88939.1), Rat AKAP7 δ/γ (NCBI RefSeq: NP_001001801.1), Mouse AKAP7 isoform-1 (NCBI RefSeq: NP_061217.3), Human AKAP7 γ (NCBI RefSeq: NP_057461.2), Human RVA WA VP3 (GenBank: AFR77808.1), Simian RVA SA11 N5 (GenBank: AFK09591.1), Human RVB Bang117 (GenBank: ADF57896.1), BtCoV SC2013 NS4b (GenBank: AHY61340.1) and BtCoV HKU5 NS4b (NCBI RefSeq: YP_001039965.1).

ACKNOWLEDGEMENTS

We thank Dr. Renliang Zhang of Mass Spectrometry Core, Lerner Research Institute, Cleveland Clinic for performing LC/MS/MS and to Kristin Ogden (Vanderbilt University)

for the rotavirus VP3-CTD cDNAs, and we thank Babal Kant Jha (Cleveland Clinic), Harpreet Kaur (Cleveland Clinic), Nikhil Bharambe (Case Western Reserve University) and Stephen A. Goldstein (University of Utah) for discussions.

FUNDING

We wish to acknowledge support by the National Institute of Allergy and Infectious Diseases of the National Institutes of Health under Awards [R01AI104887 to S.R.W. and R.H.S., AI140442 to S.R.W., and R01AI135922 to R.H.S.]

CONFLICT OF INTEREST

R.H.S. is a consultant to Inception Therapeutics, Inc., S.R.W. is on the scientific advisory board of Immunome, Inc and Ocugen, Inc.

FIGURE LEGENDS

Figure 1. Interplay between cellular responses to viral and host dsRNA, the OAS-RNase L pathway, and antagonism by 2-5A degrading enzymes. (A) OASs(1-3) are IFN induced dsRNA sensors, once activated they synthesize the antiviral substance 2',5'-oligoadenylates (2-5A) from ATP. 2-5A binds inactive monomeric RNase L inducing active RNase L dimers, which in turn degrade viral and host single-stranded RNAs. The balance between 2-5A accumulation by OAS enzymes and its degradation by host and viral enzymes determines cell and virus fate and inflammatory responses. (B) Domain structure of viral and cellular 2',5'-PEs and human PDE12 (an endonuclease/exonuclease/phosphatase (EEP) family member). Features of full length

MERS-CoV NS4b, MHV NS2, RVA SA11 VP3 and *M. musculus* AKAP7γ proteins including a nuclear localization sequence (NLS) and catalytic 2',5'-PE domains are compared, modified from ref. (24). Position of conserved histidines within the catalytic domain of 2',5'-PEs are shown. PKA-RII-α-BD, a binding domain for regulatory subunit (RII) of cAMP-dependent protein kinase A (27), guanylyltransferase (Gtase), and methyltransferase (Mtase) domains are also shown (25, 29). The mitochondrial-matrix targeting peptide (MTP) and the catalytic EEP domain of PDE12 is shown (55). Domains shown are not drawn to scale.

Figure 2. Phylogenetic relationship and sequence alignment of 2',5'-PEs. (A) Phylogenetic tree based on amino acids from catalytic domains of 2',5'-PEs is shown. The numbers represents branch length. (B) Sequence alignment of amino acids spanning the catalytic domain of 2',5'-PEs using MAFFT multiple sequence alignment program is shown. Catalytic motifs [H-Φ-(S/T)-Φ] are indicated above the boxes, where Φ represents a hydrophobic residue. Numbers represent the start and end of the amino acid sequences used for sequence alignment. Aligned residues are color-coded for conservation according to the CLUSTAL X scheme. Hydrophobic, blue; positive charge, red; negative charge, magenta; polar, green; glycine, orange; proline, yellow; aromatic, cyan; unconserved, white. Hu, human; Mu, mouse; HE, human enteric; E, equine; Bt, bat; CoV, coronavirus; RVA, rotavirus group A; RVB, rotavirus group B.

Figure 3. Specific cleavage of trimer 2-5A (2',5'-p_3A_3) by viral and cellular 2',5'-PEs. HPLC analysis of (A) intact 2',5'-p_3A_3, followed by its cleavage with either viral

2',5'-PEs (B) MERS-NS4b, (C) MHV NS2, (D) RVA VP3-CTD or a host 2',5'-PE (E) muAKAP7 or (F) human PDE12. Purified 2',5'-p_3A_3 (200 µM) was incubated with 1µM of indicated proteins at 30°C for 1 h. HPLC analysis of catalytically inactive mutants of these enzymes incubated with 2',5'-p_3A_3 under similar conditions is shown for (G) MERS-NS4b^{H182R} (H) MHV NS2^{H126R} (I) RVA VP3-CTD^{H718A} (J) muAKAP7$^{H93A;\ H185R}$ and (K) human PDE12^{E351A}. Experiments performed at least three times produced a similar 2',5'-p_3A_3 degradation pattern for each 2',5'-PEs. Arrows indicate elution times of the standards ATP, AMP, and adenosine (Ado). Peaks shown in grey were determined from experiments done in figures 5 and 6.

Figure 4. Influence of Mg^{2+} ions on degradation of 2',5'-p_3A_3 by 2',5'-PEs. Purified 2',5'-p_3A_3 was incubated with indicated 2',5'-PEs in time-course experiments. Data was obtained by incubating 2',5'-p_3A_3 (200 µM) with (A) MERS-NS4b (1µM), (B) MHV NS2 (1 µM), (C) RVA VP3-CTD (0.05 µM) and (D) muAKAP7 (1 µM) at 30°C. Samples were collected at 1, 2, 5, 10, 20 and 30 min and reactions were stopped. The percent of uncleaved 2',5'-p_3A_3 remaining at indicated times were determined by calculating the area under the peaks on the HPLC chromatograms. (E) The table shows the specific activity of 2',5'-PEs in the absence and presence of 10 mM $MgCl_2$. Activity is expressed as the amount of products released from the substrate in nMol per min per mg of the protein at 30°C during 5 min reaction time. Experiments were performed in triplicate (n = 3) and the standard error of mean was calculated.

Figure 5. MERS-NS4b cleaves 2',5'-p_3A_3 and catalyzes the formation of 2',3' cyclic phosphate products. (A) Schematic illustration of the strategy to identify the cleavage mechanism and degradation products of 2',5'-p_3A_3 by MERS-NS4b. (B) Chromatogram of partially degraded 2',5'-p_3A_3 and cleavage products formed by MERS-NS4b. 200 µM of 2',5'-p_3A_3 was incubated with 1 µM of MERS-NS4b at 30°C for 10 min. (C) HPLC chromatogram of the collected peak (corresponds to ApA). (D) HPLC chromatogram of the collected peak (corresponds to p_3A>p). (E) HPLC analysis of the dephosphorylated product (A>p) of peak collected in figure 5D (p_3A>p). (F) Schematic illustration showing shrimp alkaline phosphatase (SAP) mediated p_3A>p dephosphorylation at 5' end forms A>p. (G) Expected masses of potential 2',5'-p_3A_3 degradation products containing 3'OH, 2'p or 2',3'>p groups. Box shows masses of actual cleavage products identified by mass spectrometry. Mass spectrometry analysis showing m/z of (H) ApA → peak fraction collected in C, (I) p_3A>p → peak collected in D and (J) intact 2',5'-p_3A_3. m/z is the mass-charge ratio. Peaks shown in grey were identified in the subsequent experiments.

Figure 6. 2',5'-p_3A_3 cleavage by RVA VP3-CTD proceeds via formation of p_3ApA>p and ApA intermediates. (A) Schematic illustration of the strategy to identify the cleavage mechanism, intermediates and end products of 2',5'-p_3A_3 cleavage by RVA VP3-CTD. (B) Chromatogram of intact p_3A_3. (C) HPLC chromatogram of cleavage products formed by degradation of 200 µM 2',5'-p_3A_3 incubated with 0.05 µM of RVA VP3-CTD for 20 min at 30°C. Peaks identified based on elution times of known standards are marked. (D) HPLC analysis of the dephosphorylated products from the reaction in figure 6C. Shrimp alkaline phosphatase (SAP) treatment dephosphorylate 5'-

phosphates. The peaks indicated were collected and identified by LC/MS/MS analysis. (E) Schematic illustration showing dephosphorylation of potential intermediates at 5' end using SAP. Mass spectrometry analysis showing m/z of (F) A>p and (G) ApA>p. m/z is the mass-charge ratio. Peaks shown in grey were identified in the subsequent experiments.

Figure 7. Mechanism of 2'-5'-p_3A_3 degradation by 2',5'-PEs (a subfamily of 2H-PEs superfamily) and EEP (endonuclease/exonuclease/phosphatase) family. MERS-CoV NS4b, MHV-CoV NS2, RVA VP3, and mammalian mouse AKAP7 from the 2',5'-PE subfamily cleave 2',5'-p_3A_3 and leaves 2',3' >p groups on the 5'-products. While human PDE12, an EEP family member degrades 2',5'-p_3A_3 to yield ATP and AMP.

SUPPLEMENTARY FIGURES AND TABLES

Figure S1. 2',5'-$p(A)_5$ degradation by MHV NS2 decreases in the presence of 2',5'-$p(U)_5$. Substrate 2',5'-$p(A)_5$ was incubated with 0.2 mM of MHV-NS2 wild type protein in the absence or presence of indicated concentration of 2',5'-$p(U)_5$ at 30°C for 10 min. Samples were processed and analyzed by HPLC. 2',5'-$p(A)_5$ incubated under similar conditions in the absence of MHV-NS2 and 2',5'-$p(U)_5$ served as non-degraded control. Experiments were performed three times (n=3) and bars represent the standard error of mean. Statistical significance was calculated using unpaired t test (n=3; *, P value < 0.05; **, P < 0.005;***, P < 0.001; ns, not significant) in GraphPad Prism (9.0.0) software.

824 **Figure S2. MERS-NS4b degrades 2',5'-p_3A_3 but not 2',5' linked ApA or pApA.**
825 Substrate 2',5'-p_3A_3 (A) was degraded in the presence of NS4b into p_3A>p and ApA (B).
826 Panels B, C, and D showed no appreciable decrease in amounts of ApA (area under
827 the peak) after incubation for 1, 4 and 24 h, respectively. Panels E, F, G and H shows
828 HPLC chromatograms of substrate pApA in the presence for NS4b at 0, 1, 4 and 24 h.
829 (I) The table shows the amount of ApA or pApA degraded by NS4b as a function of
830 time.

831

832 **Figure S3. Time-course of 2',5'-p_3A_3 cleavage by RVA VP3-CTD.** Purified 2',5'-p_3A_3
833 (200 µM) was incubated with RVA VP3-CTD (0.05 µM) at 30°C. Samples were collected
834 at (A) 0 min, (B) 2 min, (C) 5 min, (D) 10 min, and (E) 30 min and analyzed by HPLC.
835 The percent of substrate or products at indicated times were determined by calculating
836 the area under the peaks on the HPLC chromatograms. Right hand side shows major
837 and minor reactions proceeding at the indicated time points deduced from HPLC
838 chromatogram analysis.

839

840 **Figure S4. Mechanism of 2',5'-p_3A_3 cleavage by RVA VP3-CTD.** (A) The percentage
841 of the substrate or the products at indicated times were determined by calculating the
842 area under the peaks on the HPLC chromatograms obtained in experiment from figure
843 S3. (B) Summary of major and minor reactions involved in cleavage of 2',5'-p_3A_3 by
844 VP3-CTD. The minor reaction cleavage of ApA to A>p and Ado is inferred from

incubations performed at a 20-fold higher concentration of RVA VP3-CTD, 1 mM (Fig. 3D).

Figure S5. RVA VP3-CTD degrades 2',5' linked di-adenylate. (A) Substrate 2',5'-pApA (A) was incubated with 1 mM of either (B) wild type RVA VP3-CTD or its mutant (C) RVA VP3 CTDH^{718A} at 30°C for 1 h. Samples were processed and analyzed by HPLC. Baseline buffer signal was subtracted from the samples.

Figure S6. Time-course of 2',5'-p_3A_3 cleavage by muAKAP7. Purified 2',5'-p_3A_3 (200 µM) was incubated with muAKAP7 (1 µM) at 30°C. Samples were collected at (A) 0 min, (B) 2 min, (C) 10 min, (D) 30 min and (E) 60 min and analyzed by HPLC. The peaks were identified by comparing the elution time of known standards. The percent of substrate or products at indicated times were determined by calculating the area under the peaks on the HPLC chromatograms. (F) Schematics showing cleavage of 2',5'-p_3A_3 by muAKAP7. Reaction intermediate is shown in grey color.

Table S1. Catalytic domain sequence identity and similarity analysis of viral and cellular 2',5'-PEs. Percent amino acid identity and similarity matrix is based on alignment in figure 2B. 2',5'-PEs from mammals or mammalian viruses were used for alignment. Values are calculated using Sequence Identity and Similarity (SIAS) tool. Matrix values show percent identity (above diagonal) and similarity (below diagonal)

between the corresponding pair of the proteins. Intragroup identity and similarity values are shaded in grey.

Table S2. MERS-NS4b, MHV NS2, RVA VP3-CTD and muAKAP7 mediated degradation of 5'-phosphorylated, 2'-5' or 3'-5' linked penta-ribonucleotide substrates. Ten µM of the indicated substrate was incubated with 1 µM of wild type or mutant 2',5'-PE for 1 h at 30°C. Percent substrate degradation was calculated by measuring the area under the peaks in the HPLC chromatograms. Results were reproduced in at least two independent experiments.

Table S3. MERS-NS4b mediated degradation of 5'-phosphorylated 2'-5' or 3'-5' linked penta-ribonucleotide substrates. Ten µM of the indicated substrate was incubated with 3 µM of wild type or mutant MERS-NS4b for 1 h at 30°C. Percent substrate degradation was calculated by measuring the area under the peaks in the HPLC chromatograms. Results were reproduced in two independent experiments.

Table S4. 2',5'-PEs mediated degradation of 2',3'-cGAMP and 2',5'-p_3A_3. Ten µM of the indicated substrate was incubated with 1 µM of wild type or mutant 2',5'-PEs for 1 h at 30°C. Substrate without enzyme incubated under similar condition were used as un-degraded control. Percent substrate degradation was calculated by measuring the area under the peaks in the HPLC chromatograms. Results were reproduced in two independent experiments.

888

889

REFERENCES

1. Borden EC, Sen GC, Uze G, Silverman RH, Ransohoff RM, Foster GR, Stark GR. 2007. Interferons at age 50: past, current and future impact on biomedicine. Nat Rev Drug Discov 6:975-90.
2. Samuel CE. 2001. Antiviral actions of interferons. Clin Microbiol Rev 14:778-809, table of contents.
3. Weiss SR. 2020. Forty years with coronaviruses. J Exp Med 217.
4. Li Y, Renner DM, Comar CE, Whelan JN, Reyes HM, Cardenas-Diaz FL, Truitt R, Tan LH, Dong B, Alysandratos KD, Huang J, Palmer JN, Adappa ND, Kohanski MA, Kotton DN, Silverman RH, Yang W, Morrisey E, Cohen NA, Weiss SR. 2020. SARS-CoV-2 induces double-stranded RNA-mediated innate immune responses in respiratory epithelial derived cells and cardiomyocytes. Proc Natl Acad Sci U S A (in press) DOI: 10.1073/pnas.2022643118.
5. Der SD, Zhou A, Williams BR, Silverman RH. 1998. Identification of genes differentially regulated by interferon alpha, beta, or gamma using oligonucleotide arrays. Proc Natl Acad Sci U S A 95:15623-8.
6. Hovanessian AG, Brown RE, Kerr IM. 1977. Synthesis of low molecular weight inhibitor of protein synthesis with enzyme from interferon-treated cells. Nature 268:537-40.
7. Kerr IM, Brown RE. 1978. pppA2'p5'A2'p5'A: an inhibitor of protein synthesis synthesized with an enzyme fraction from interferon-treated cells. Proc Natl Acad Sci U S A 75:256-60.
8. Kristiansen H, Gad HH, Eskildsen-Larsen S, Despres P, Hartmann R. 2011. The oligoadenylate synthetase family: an ancient protein family with multiple antiviral activities. J Interferon Cytokine Res 31:41-7.
9. Kakuta S, Shibata S, Iwakura Y. 2002. Genomic structure of the mouse 2',5'-oligoadenylate synthetase gene family. J Interferon Cytokine Res 22:981-93.
10. Li Y, Dong B, Wei Z, Silverman RH, Weiss SR. 2019. Activation of RNase L in Egyptian Rousette Bat-Derived RoNi/7 Cells Is Dependent Primarily on OAS3 and Independent of MAVS Signaling. mBio 10.
11. Clemens MJ, Williams BR. 1978. Inhibition of cell-free protein synthesis by pppA2'p5'A2'p5'A: a novel oligonucleotide synthesized by interferon-treated L cell extracts. Cell 13:565-72.
12. Zhou A, Hassel BA, Silverman RH. 1993. Expression cloning of 2-5A-dependent RNAase: a uniquely regulated mediator of interferon action. Cell 72:753-65.
13. Castelli JC, Hassel BA, Wood KA, Li XL, Amemiya K, Dalakas MC, Torrence PF, Youle RJ. 1997. A study of the interferon antiviral mechanism: apoptosis activation by the 2-5A system. J Exp Med 186:967-72.
14. Zhou A, Paranjape J, Brown TL, Nie H, Naik S, Dong B, Chang A, Trapp B, Fairchild R, Colmenares C, Silverman RH. 1997. Interferon action and apoptosis are defective in mice devoid of 2',5'-oligoadenylate-dependent RNase L. EMBO J 16:6355-63.

15. Chakrabarti A, Banerjee S, Franchi L, Loo YM, Gale M, Jr., Nunez G, Silverman RH. 2015. RNase L activates the NLRP3 inflammasome during viral infections. Cell Host Microbe 17:466-77.
16. Li Y, Banerjee S, Goldstein SA, Dong B, Gaughan C, Rath S, Donovan J, Korennykh A, Silverman RH, Weiss SR. 2017. Ribonuclease L mediates the cell-lethal phenotype of double-stranded RNA editing enzyme ADAR1 deficiency in a human cell line. Elife 6.
17. Banerjee S, Gusho E, Gaughan C, Dong B, Gu X, Holvey-Bates E, Talukdar M, Li Y, Weiss SR, Sicheri F, Sauntharajah Y, Stark GR, Silverman RH. 2019. OAS-RNase L innate immune pathway mediates the cytotoxicity of a DNA-demethylating drug. Proc Natl Acad Sci U S A 116:5071-5076.
18. Mehdipour P, Marhon SA, Ettayebi I, Chakravarthy A, Hosseini A, Wang Y, de Castro FA, Loo Yau H, Ishak C, Abelson S, O'Brien CA, De Carvalho DD. 2020. Epigenetic therapy induces transcription of inverted SINEs and ADAR1 dependency. Nature 588:169-173.
19. Mazumder R, Iyer LM, Vasudevan S, Aravind L. 2002. Detection of novel members, structure-function analysis and evolutionary classification of the 2H phosphoesterase superfamily. Nucleic Acids Res 30:5229-43.
20. Silverman RH, Weiss SR. 2014. Viral phosphodiesterases that antagonize double-stranded RNA signaling to RNase L by degrading 2-5A. J Interferon Cytokine Res 34:455-63.
21. Nomura Y, Roston D, Montemayor EJ, Cui Q, Butcher SE. 2018. Structural and mechanistic basis for preferential deadenylation of U6 snRNA by Usb1. Nucleic Acids Res 46:11488-11501.
22. Zhao L, Jha BK, Wu A, Elliott R, Ziebuhr J, Gorbalenya AE, Silverman RH, Weiss SR. 2012. Antagonism of the interferon-induced OAS-RNase L pathway by murine coronavirus ns2 protein is required for virus replication and liver pathology. Cell Host Microbe 11:607-16.
23. Goldstein SA, Thornbrough JM, Zhang R, Jha BK, Li Y, Elliott R, Quiroz-Figueroa K, Chen AI, Silverman RH, Weiss SR. 2017. Lineage A Betacoronavirus NS2 Proteins and the Homologous Torovirus Berne pp1a Carboxy-Terminal Domain Are Phosphodiesterases That Antagonize Activation of RNase L. J Virol 91.
24. Thornbrough JM, Jha BK, Yount B, Goldstein SA, Li Y, Elliott R, Sims AC, Baric RS, Silverman RH, Weiss SR. 2016. Middle East Respiratory Syndrome Coronavirus NS4b Protein Inhibits Host RNase L Activation. mBio 7:e00258.
25. Zhang R, Jha BK, Ogden KM, Dong B, Zhao L, Elliott R, Patton JT, Silverman RH, Weiss SR. 2013. Homologous 2',5'-phosphodiesterases from disparate RNA viruses antagonize antiviral innate immunity. Proc Natl Acad Sci U S A 110:13114-9.
26. Song Y, Feng N, Sanchez-Tacuba L, Yasukawa LL, Ren L, Silverman RH, Ding S, Greenberg HB. 2020. Reverse Genetics Reveals a Role of Rotavirus VP3 Phosphodiesterase Activity in Inhibiting RNase L Signaling and Contributing to Intestinal Viral Replication In Vivo. J Virol 94.
27. Gusho E, Zhang R, Jha BK, Thornbrough JM, Dong B, Gaughan C, Elliott R, Weiss SR, Silverman RH. 2014. Murine AKAP7 has a 2',5'-phosphodiesterase

domain that can complement an inactive murine coronavirus ns2 gene. mBio 5:e01312-14.

28. Canton J, Fehr AR, Fernandez-Delgado R, Gutierrez-Alvarez FJ, Sanchez-Aparicio MT, Garcia-Sastre A, Perlman S, Enjuanes L, Sola I. 2018. MERS-CoV 4b protein interferes with the NF-kappaB-dependent innate immune response during infection. PLoS Pathog 14:e1006838.
29. Chen D, Luongo CL, Nibert ML, Patton JT. 1999. Rotavirus open cores catalyze 5'-capping and methylation of exogenous RNA: evidence that VP3 is a methyltransferase. Virology 265:120-30.
30. Ogden KM, Snyder MJ, Dennis AF, Patton JT. 2014. Predicted structure and domain organization of rotavirus capping enzyme and innate immune antagonist VP3. J Virol 88:9072-85.
31. Kindler E, Trojnar E, Heckel G, Otto PH, Johne R. 2013. Analysis of rotavirus species diversity and evolution including the newly determined full-length genome sequences of rotavirus F and G. Infect Genet Evol 14:58-67.
32. Kubota K, Nakahara K, Ohtsuka T, Yoshida S, Kawaguchi J, Fujita Y, Ozeki Y, Hara A, Yoshimura C, Furukawa H, Haruyama H, Ichikawa K, Yamashita M, Matsuoka T, Iijima Y. 2004. Identification of 2'-phosphodiesterase, which plays a role in the 2-5A system regulated by interferon. J Biol Chem 279:37832-41.
33. Poulsen JB, Andersen KR, Kjaer KH, Vestergaard AL, Justesen J, Martensen PM. 2012. Characterization of human phosphodiesterase 12 and identification of a novel 2'-5' oligoadenylate nuclease - The ectonucleotide pyrophosphatase/phosphodiesterase 1. Biochimie 94:1098-107.
34. Rorbach J, Nicholls TJ, Minczuk M. 2011. PDE12 removes mitochondrial RNA poly(A) tails and controls translation in human mitochondria. Nucleic Acids Res 39:7750-63.
35. Hopfner KP, Hornung V. 2020. Molecular mechanisms and cellular functions of cGAS-STING signalling. Nat Rev Mol Cell Biol 21:501-521.
36. Romani AM. 2011. Cellular magnesium homeostasis. Arch Biochem Biophys 512:1-23.
37. Dong B, Xu L, Zhou A, Hassel BA, Lee X, Torrence PF, Silverman RH. 1994. Intrinsic molecular activities of the interferon-induced 2-5A-dependent RNase. J Biol Chem 269:14153-8.
38. Kondratova AA, Cheon H, Dong B, Holvey-Bates EG, Hasipek M, Taran I, Gaughan C, Jha BK, Silverman RH, Stark GR. 2020. Suppressing PARylation by 2',5'-oligoadenylate synthetase 1 inhibits DNA damage-induced cell death. EMBO J 39:e101573.
39. Ferbus D, Justesen J, Besancon F, Thang MN. 1981. The 2'5' oligoadenylate synthetase has a multifunctional 2'5' nucleotidyl-transferase activity. Biochem Biophys Res Commun 100:847-56.
40. Justesen J, Hartmann R, Kjeldgaard NO. 2000. Gene structure and function of the 2'-5'-oligoadenylate synthetase family. Cell Mol Life Sci 57:1593-612.
41. Cayley PJ, Kerr IM. 1982. Synthesis, characterisation and biological significance of (2'-5')oligoadenylate derivatives of NAD+, ADP-ribose and adenosine(5')tetraphospho(5')adenosine. Eur J Biochem 122:601-8.

42. Cooper DA, Jha BK, Silverman RH, Hesselberth JR, Barton DJ. 2014. Ribonuclease L and metal-ion-independent endoribonuclease cleavage sites in host and viral RNAs. Nucleic Acids Res 42:5202-16.
43. Lopp A, Reintamm T, Kuusksalu A, Olspert A, Kelve M. 2019. Identification of a novel member of 2H phosphoesterases, 2',5'-oligoadenylate degrading ribonuclease from the oyster Crassostrea gigas. Biochimie 156:181-195.
44. Malathi K, Dong B, Gale M, Jr., Silverman RH. 2007. Small self-RNA generated by RNase L amplifies antiviral innate immunity. Nature 448:816-9.
45. Greulich W, Wagner M, Gaidt MM, Stafford C, Cheng Y, Linder A, Carell T, Hornung V. 2019. TLR8 Is a Sensor of RNase T2 Degradation Products. Cell 179:1264-1275 e13.
46. Garcia-Sastre A. 2017. Ten Strategies of Interferon Evasion by Viruses. Cell Host Microbe 22:176-184.
47. Wood ER, Bledsoe R, Chai J, Daka P, Deng H, Ding Y, Harris-Gurley S, Kryn LH, Nartey E, Nichols J, Nolte RT, Prabhu N, Rise C, Sheahan T, Shotwell JB, Smith D, Tai V, Taylor JD, Tomberlin G, Wang L, Wisely B, You S, Xia B, Dickson H. 2015. The Role of Phosphodiesterase 12 (PDE12) as a Negative Regulator of the Innate Immune Response and the Discovery of Antiviral Inhibitors. J Biol Chem 290:19681-96.
48. Chung H, Calis JJA, Wu X, Sun T, Yu Y, Sarbanes SL, Dao Thi VL, Shilvock AR, Hoffmann HH, Rosenberg BR, Rice CM. 2018. Human ADAR1 Prevents Endogenous RNA from Triggering Translational Shutdown. Cell 172:811-824 e14.
49. Leonova KI, Brodsky L, Lipchick B, Pal M, Novototskaya L, Chenchik AA, Sen GC, Komarova EA, Gudkov AV. 2013. p53 cooperates with DNA methylation and a suicidal interferon response to maintain epigenetic silencing of repeats and noncoding RNAs. Proc Natl Acad Sci U S A 110:E89-98.
50. Tyagi R, Lai R, Duggleby RG. 2004. A new approach to 'megaprimer' polymerase chain reaction mutagenesis without an intermediate gel purification step. BMC Biotechnol 4:2.
51. Estrella MA, Du J, Korennykh A. 2018. Crystal Structure of Human Nocturnin Catalytic Domain. Sci Rep 8:16294.
52. Hartmann R, Justesen J, Sarkar SN, Sen GC, Yee VC. 2003. Crystal structure of the 2'-specific and double-stranded RNA-activated interferon-induced antiviral protein 2'-5'-oligoadenylate synthetase. Mol Cell 12:1173-85.
53. Rusch L, Dong B, Silverman RH. 2001. Monitoring activation of ribonuclease L by 2',5'-oligoadenylates using purified recombinant enzyme and intact malignant glioma cells. Methods Enzymol 342:10-20.
54. Katoh K, Standley DM. 2013. MAFFT multiple sequence alignment software version 7: improvements in performance and usability. Mol Biol Evol 30:772-80.
55. Poulsen JB, Andersen KR, Kjaer KH, Durand F, Faou P, Vestergaard AL, Talbo GH, Hoogenraad N, Brodersen DE, Justesen J, Martensen PM. 2011. Human 2'-phosphodiesterase localizes to the mitochondrial matrix with a putative function in mitochondrial RNA turnover. Nucleic Acids Res 39:3754-70.

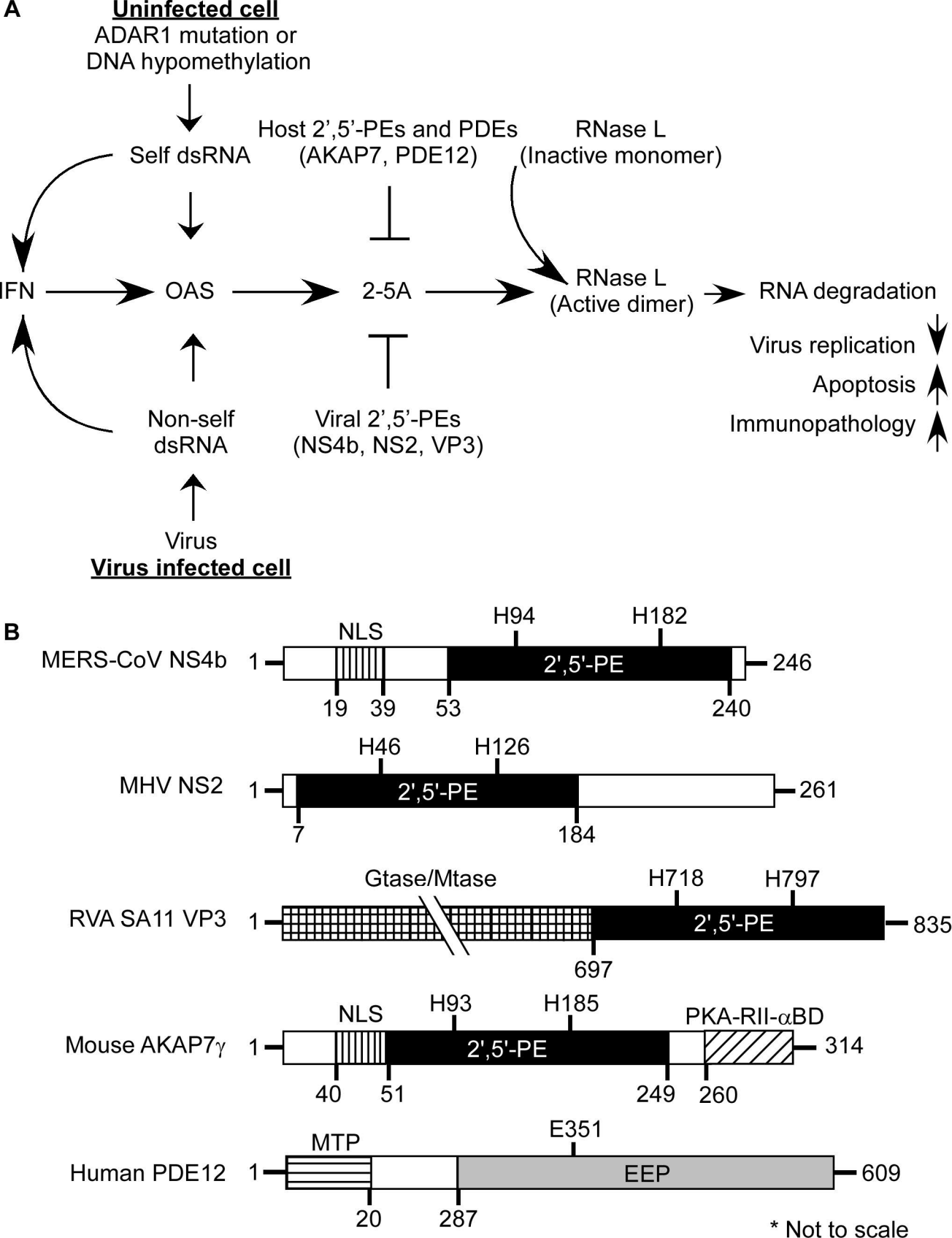
A
Uninfected cell
ADAR1 mutation or
DNA hypomethylation
Self dsRNA
Host 2',5'-PEs and PDEs
(AKAP7, PDE12)
RNase L
(Inactive monomer)
IFN
OAS
2-5A
RNase L
(Active dimer)
RNA degradation
Virus replication
Apoptosis
Immunopathology
Non-self
dsRNA
Viral 2',5'-PEs
(NS4b, NS2, VP3)
Virus
Virus infected cell
B
MERS-CoV NS4b
NLS
H94
H182
2',5'-PE
1
246
19
39
53
240
MHV NS2
H46
H126
2',5'-PE
1
261
7
184
RVA SA11 VP3
Gtase/Mtase
H718
H797
2',5'-PE
1
835
697
Mouse AKAP7γ
NLS
H93
H185
PKA-RII-αBD
2',5'-PE
1
314
40
51
249
260
Human PDE12
MTP
E351
EEP
1
609
20
287
* Not to scale

A

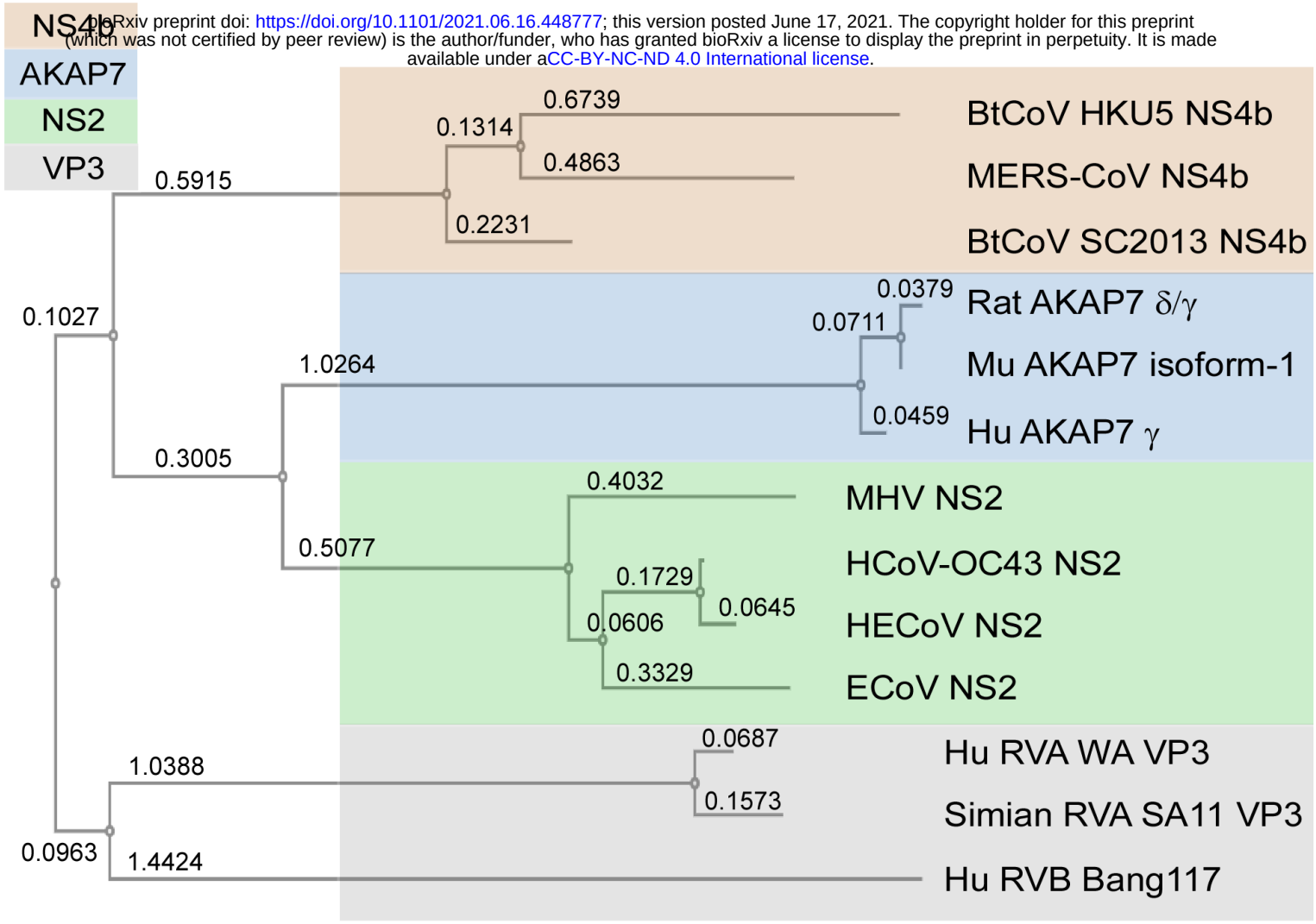

B

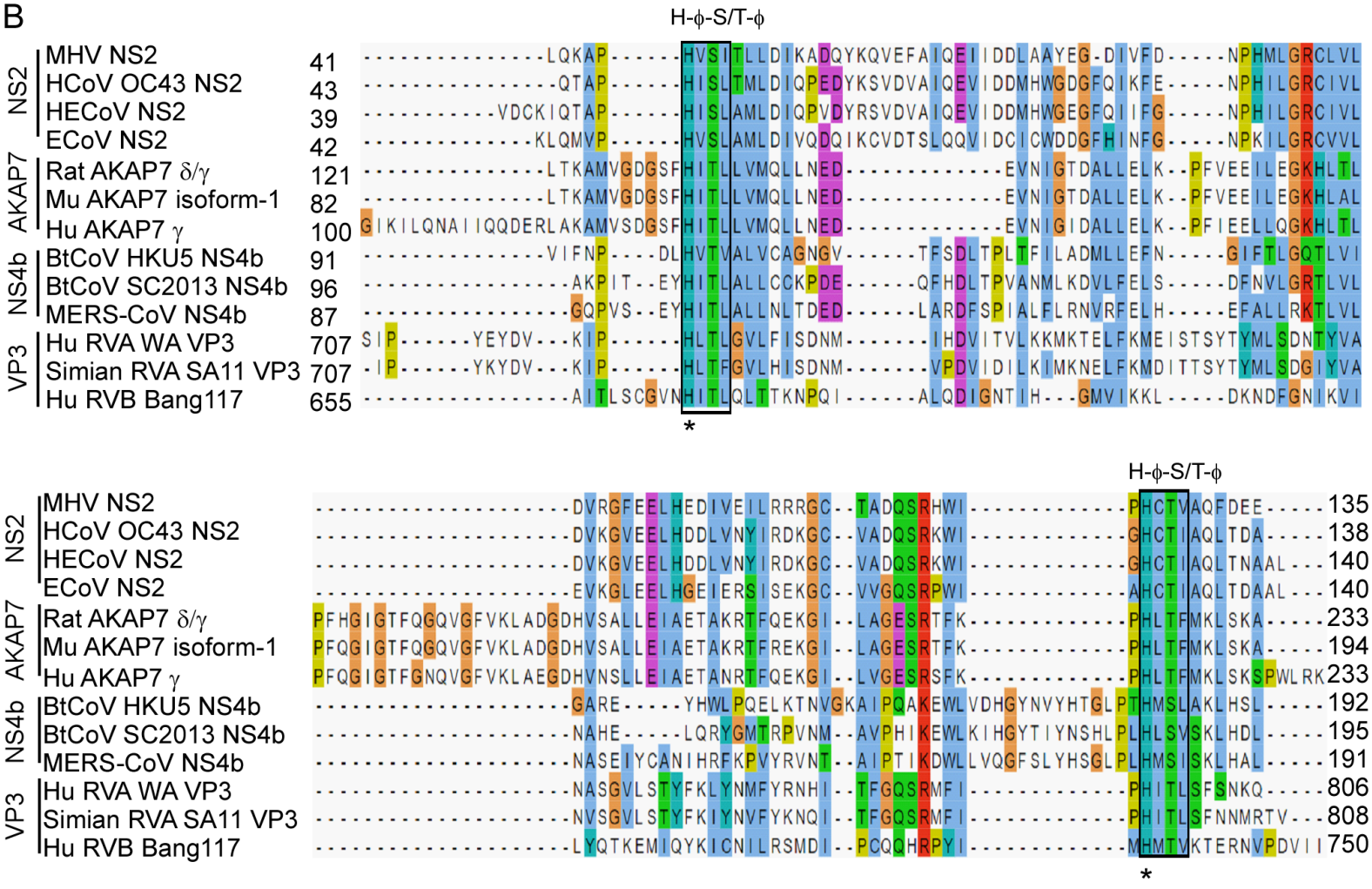

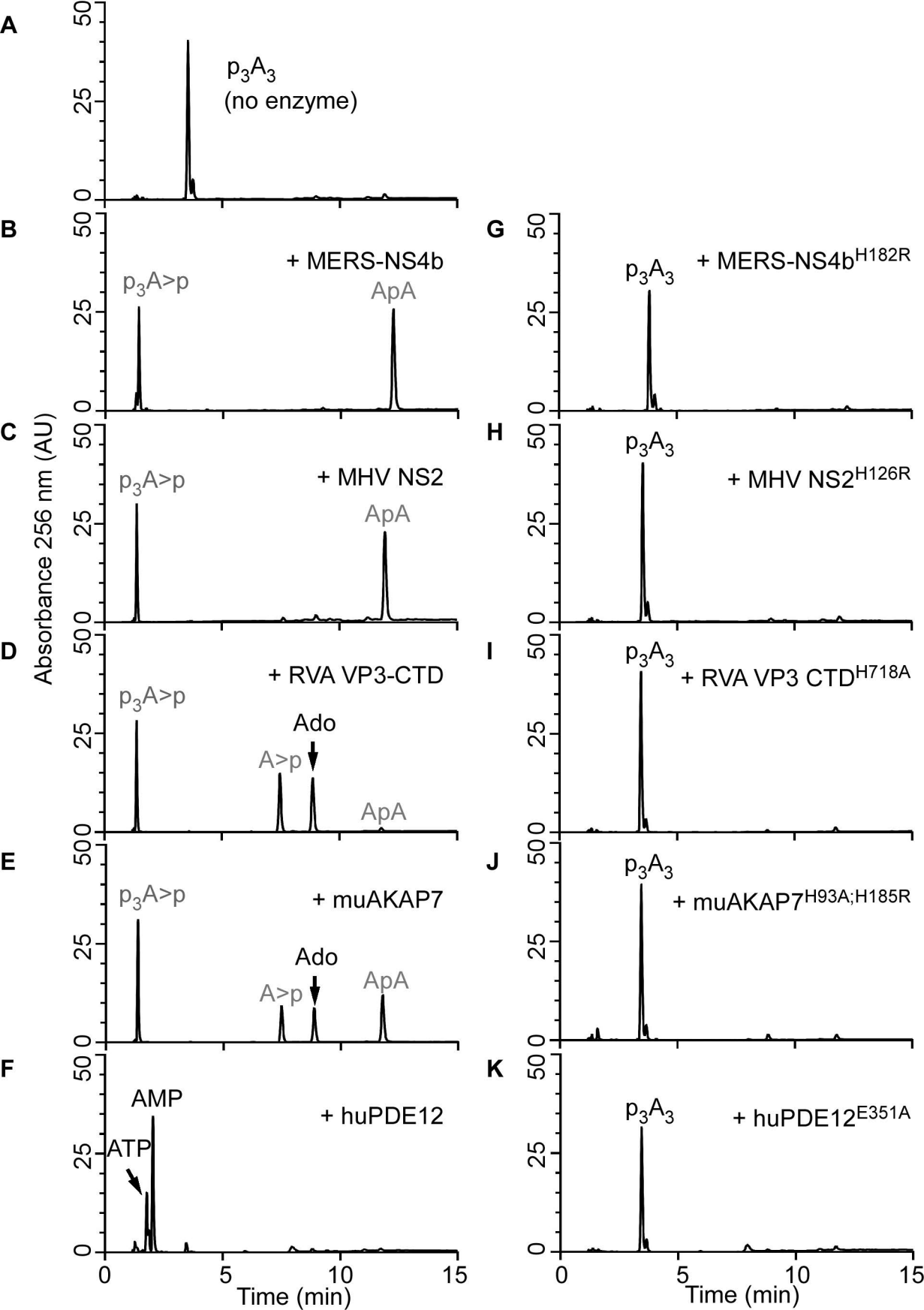
A
p_3A_3
(no enzyme)
B
+ MERS-NS4b
$p_3A>p$
ApA
C
+ MHV NS2
$p_3A>p$
ApA
D
+ RVA VP3-CTD
$p_3A>p$
Ado
A>p
ApA
E
+ muAKAP7
$p_3A>p$
Ado
A>p
ApA
F
+ huPDE12
AMP
ATP
G
+ MERS-NS4b^{H182R}
p_3A_3
H
+ MHV NS2^{H126R}
p_3A_3
I
+ RVA VP3 CTD^{H718A}
p_3A_3
J
+ muAKAP7$^{H93A;H185R}$
p_3A_3
K
+ huPDE12^{E351A}
p_3A_3
Absorbance 256 nm (AU)
0
25
50
0
5
10
15
Time (min)

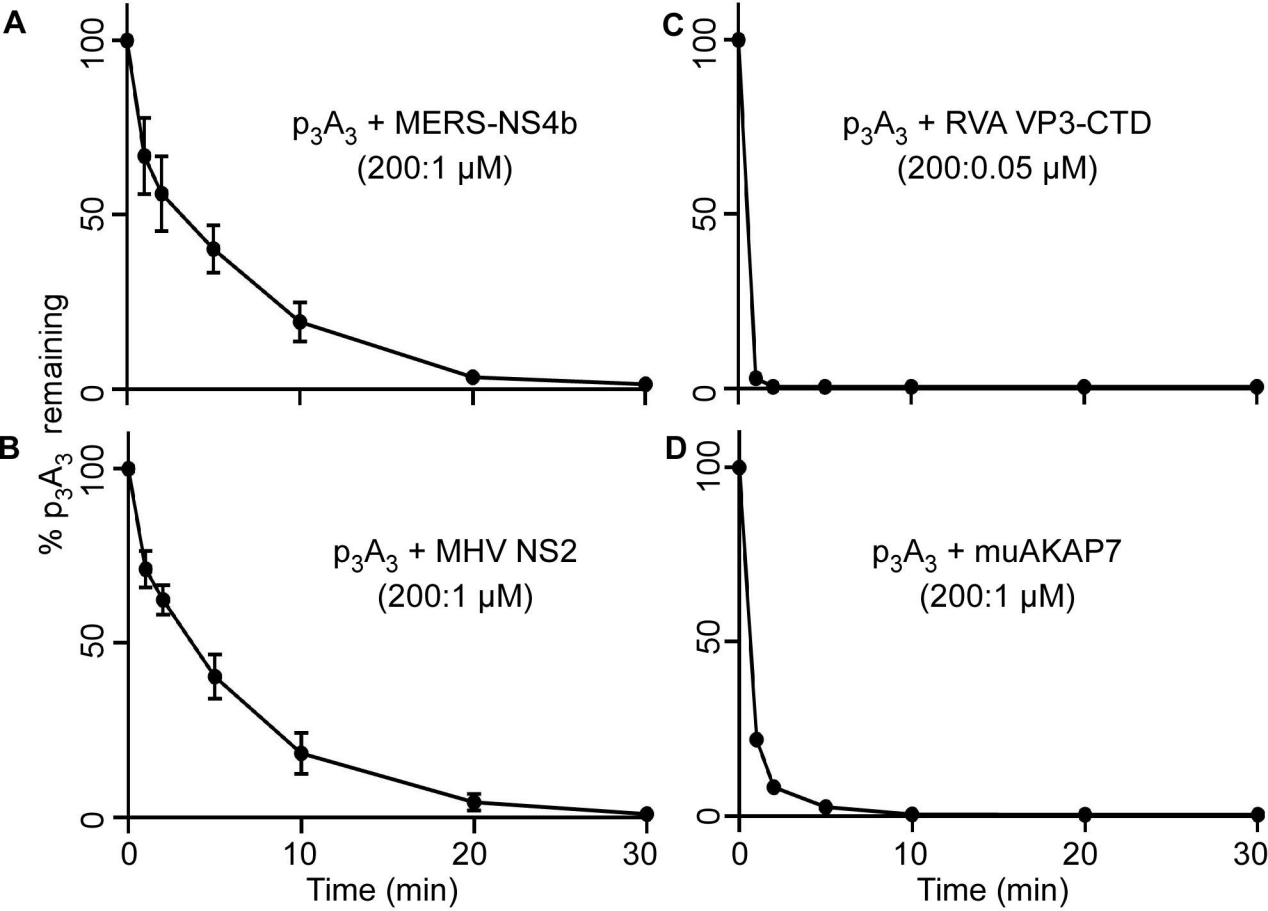

E

Protein	Specific activity (nMol-min^{-1}-mg^{-1})		
	-	+ Mg^{2+}	Specific activity ratio -/+ Mg^{2+}
MERS-NS4b	1707 ±112	1027 ±123	1.66 ±0.226
MHV NS2	1702 ±105	1666 ±123	1.02 ±0.098
RVA VP3-CTD	66339 ±10	65694 ±318	1.00 ±0.004
muAKAP7	4869 ±18	3919 ±11	1.24 ±0.005

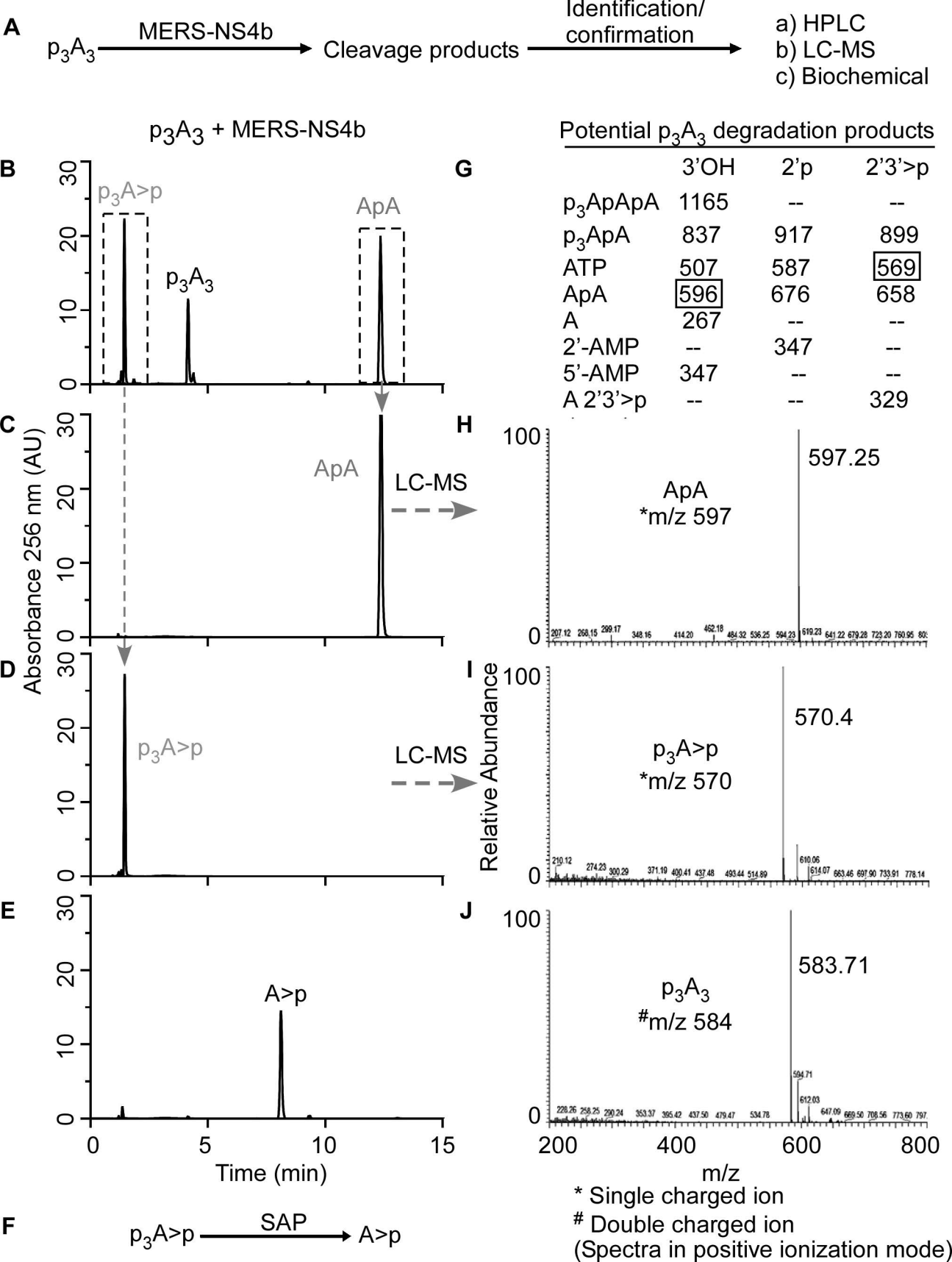
A
p3A3
MERS-NS4b
Cleavage products
Identification/ confirmation
a) HPLC
b) LC-MS
c) Biochemical
p3A3 + MERS-NS4b
B
p3A>p
ApA
p3A3
C
ApA
LC-MS
Absorbance 256 nm (AU)
D
p3A>p
LC-MS
E
A>p
Time (min)
F
p3A>p
SAP
A>p
G
Potential p3A3 degradation products
3'OH 2'p 2'3'>p
p3ApApA 1165 -- --
p3ApA 837 917 899
ATP 507 587 569
ApA 596 676 658
A 267 -- --
2'-AMP -- 347 --
5'-AMP 347 -- --
A 2'3'>p -- -- 329
H
ApA
*m/z 597
597.25
I
p3A>p
*m/z 570
570.4
Relative Abundance
J
p3A3
#m/z 584
583.71
m/z
* Single charged ion
# Double charged ion
(Spectra in positive ionization mode)

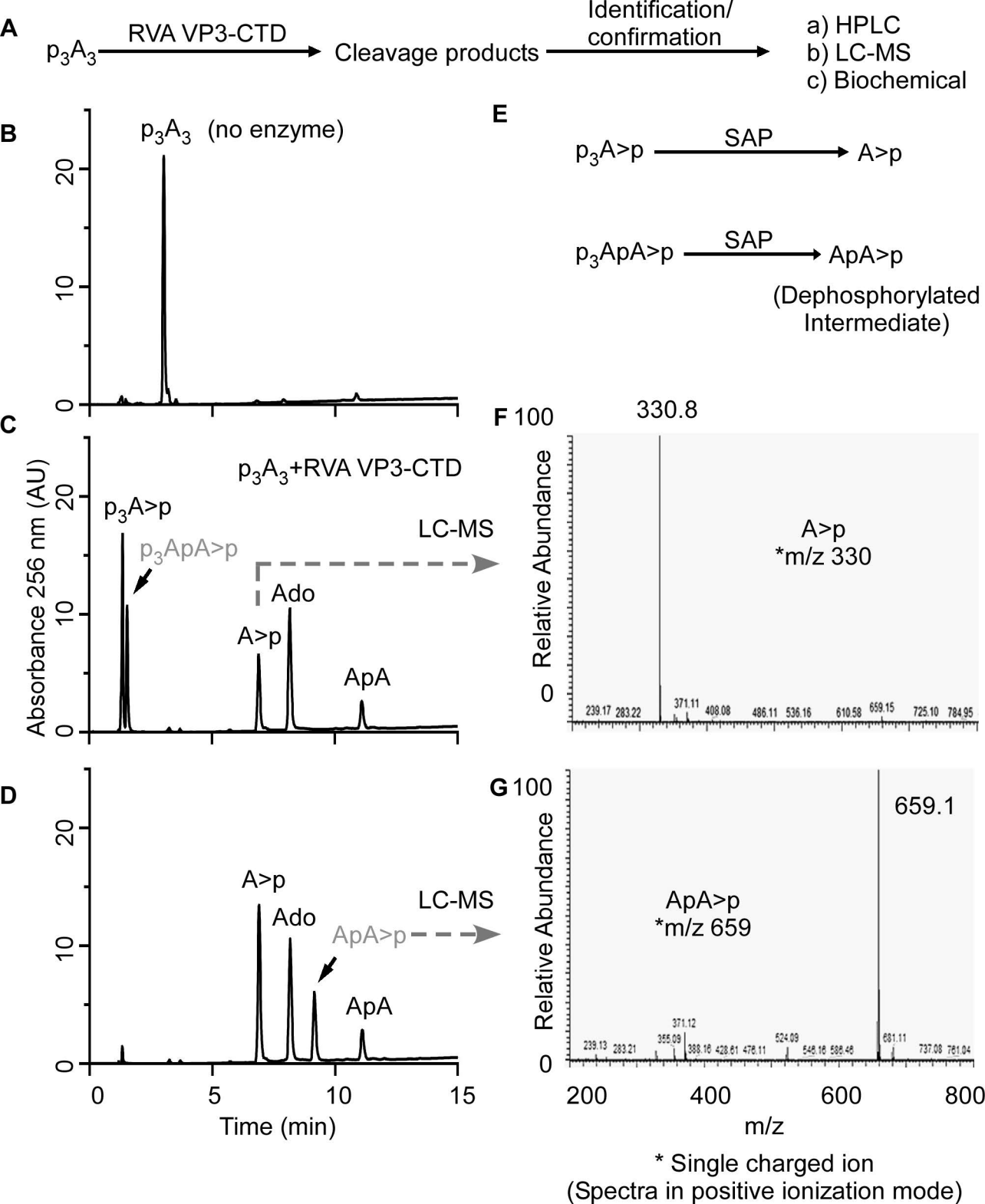
A
p3A3
RVA VP3-CTD
Cleavage products
Identification/ confirmation
a) HPLC
b) LC-MS
c) Biochemical
B
p3A3 (no enzyme)
C
p3A3+RVA VP3-CTD
p3A>p
p3ApA>p
LC-MS
Ado
A>p
ApA
Absorbance 256 nm (AU)
D
A>p
Ado
LC-MS
ApA>p
ApA
Time (min)
E
p3A>p
SAP
A>p
p3ApA>p
SAP
ApA>p
(Dephosphorylated Intermediate)
F
330.8
Relative Abundance
A>p
*m/z 330
G
659.1
ApA>p
*m/z 659
m/z
* Single charged ion
(Spectra in positive ionization mode)

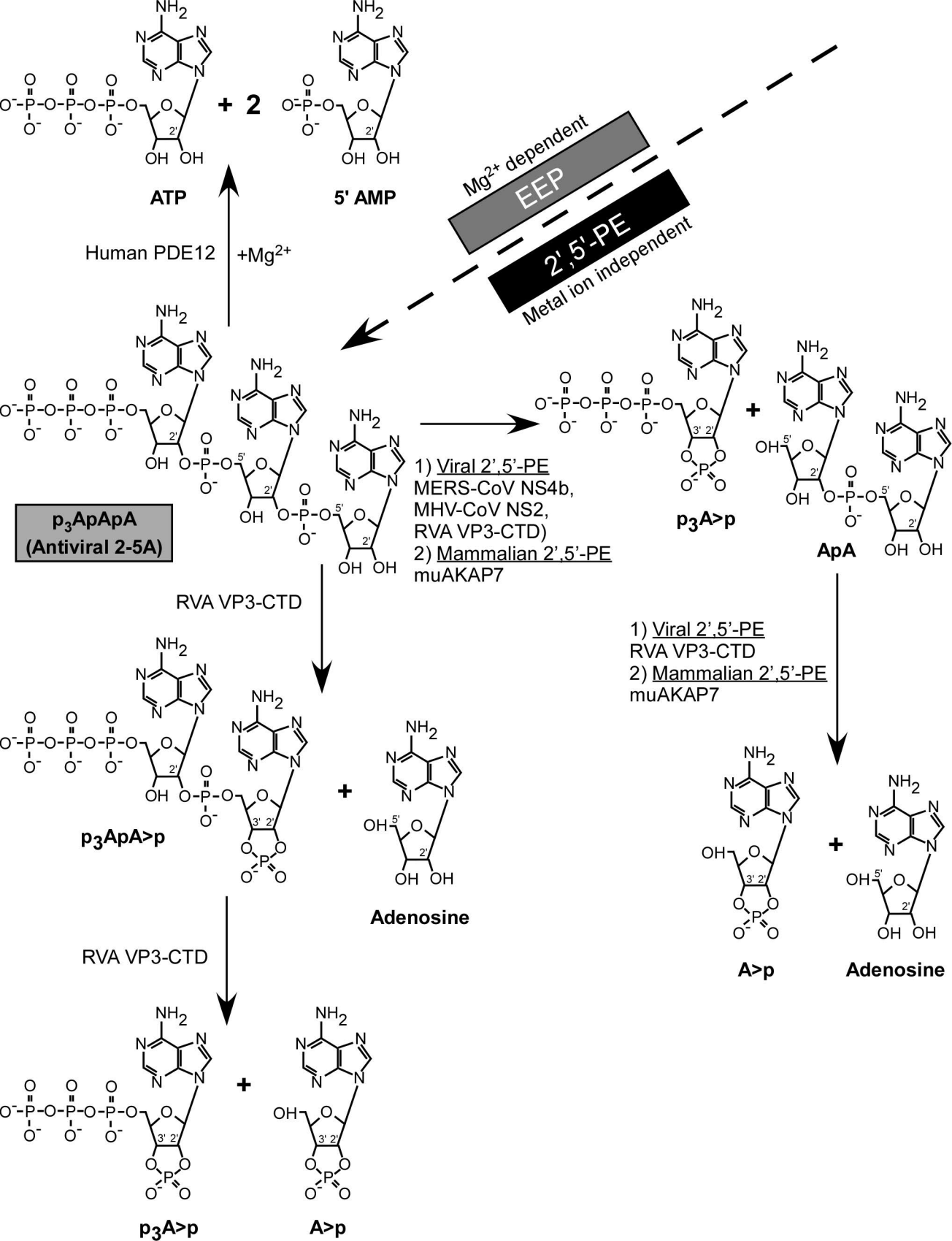
ATP
+ 2
5' AMP
Mg2+ dependent
EEP
2',5'-PE
Metal ion independent
Human PDE12
+Mg2+
p3ApApA
(Antiviral 2-5A)
1) Viral 2',5'-PE
MERS-CoV NS4b,
MHV-CoV NS2,
RVA VP3-CTD)
2) Mammalian 2',5'-PE
muAKAP7
p3A>p
ApA
RVA VP3-CTD
1) Viral 2',5'-PE
RVA VP3-CTD
2) Mammalian 2',5'-PE
muAKAP7
p3ApA>p
Adenosine
A>p
Adenosine
RVA VP3-CTD
p3A>p
A>p